A novel evaluation method of measurement sensitivities on common faults in VAV HVAC systems

Yimin Chen [a,*], Zhelun Chen [b], Guanjing Lin [c], Yun Zhang [d], Shi Ye [e]

[a] *Building Technology and Urban Systems Division, Lawrence Berkeley National Laboratory, 1 Cyclotron Road, Berkeley, CA, 94720 USA*
[b] *Department of Civil, Architectural and Environmental Engineering, Drexel University, 3141 Chestnut Street, Philadelphia, PA 19104 USA*
[c] *Tsinghua Shenzhen International Graduate School, Tsinghua University, Nanshan, Shenzhen, 518071 China*
[d] *Turntide Technologies, 1295 Forgewood Ave., Sunnyvale, CA 94089 USA*
[e] *Merck & Co, 126 E Lincoln Ave, Rahway, NJ 07065 USA*

ABSTRACT

Today, a high volume of operation interval data can be efficiently captured by a diverse range of measurements including sensors, control signals and meters, which are deployed in building automation systems (BAS). Hence, advanced data analytics tools such as fault detection and diagnostic (FDD) can be developed to analyze the operational performance of heating, ventilation and air conditioning (HVAC) systems. In the past, enormous efforts have been made to develop various FDD approaches, assuming interval data contains essential information for identifying fault signatures. However, a "data rich, but information poor" phenomenon exists due to the fact that not all measurements are sensitive to faults in HVAC systems. This highlights a significant research gap, the lack of systematic analysis of measurement sensitivity to different HVAC system faults, which is vital for FDD development, measurement deployment optimization, and control system design. To address this gap, this study introduces a novel approach to assess the sensitivity of BAS measurements in relation to various HVAC fault types. We propose two sensitivity indices (SI), the SI of fault (SI_fault) and the global measurement SI (SI_measurement_global) to quantify measurement sensitivities. The SI_fault quantifies the measurement's sensitivity to a particular fault, while the SI_measurement_global assesses its sensitivity across all fault types. These indices integrate probability distributions, enhancing the interpretability and scalability. Utilizing the HVACSIM+ fault simulation dataset, which includes 15 common faults at varying severity levels and 89 different measurements within an HVAC system, we conducted an extensive analysis of measurement sensitivities by looking at the proposed SIs.

1. Introduction

In buildings, heating, ventilation and air conditioning (HVAC) systems are used to provide desired thermal comforts and indoor air quality for occupants. HVAC systems consume a large portion of energy to achieve operational objectives. Based on the Energy Information Administration (EIA) of the U.S, HVAC systems in commercial buildings in the U.S. account for around 44% total electricity consumption [1]. In an HVAC system, various hardware related faults and software related faults cause dramatic degradation of system operational performance, and consequently lead to substantial energy wastes. Studies show that 5–30% energy wastes in commercial buildings are caused by various faults in HVAC systems in the U.S [2]. Additionally, faults can lead to

degradation of the indoor thermal comfort, as well as increased operation and maintenance costs [3–5].

The operation interval data in HVAC systems is crucial to indicate system' operation status. Today, an efficient data acquisition is empowered by the deployment of building automation systems (BAS). Consequently, in recent years, extensive studies have been carried out to develop various data-driven fault detection and diagnostics (FDD) approaches to detect and diagnose faults in HVAC systems [6–9]. Additionally, other emerging technologies, such as digital twin, have been developed to utilize operation interval data to promote knowledge discovery and enhance FDD capabilities for HVAC systems [10,11].

The successful application of data-driven FDD solutions requires certain measurements in the BASs to be sensitive to faults, so that faulty

information can be effectively captured and used by those FDD solutions. However, the dilemma of "data rich, but information poor" always exists [12,13] because measurements may not be sensitive to faults.

1.1. Motivations

A high volume of system operation data can be easily collected by a variety of measurements in the BAS [14]. For example, Chen et al. reported that around 30 measurements (e.g., temperature and humidity sensors, and valve control signals) were employed to monitor one piece of single-duct air handling unit (AHU) [15]. Additionally, it is reported that more than 500 measurements are integrated to the BAS to monitor an HVAC system, which contains a primary cooling system (i.e., a chiller plant), a heating system (i.e., a boiler plant), and three air distribution systems (including three AHUs and 88 associated variable air volume (VAV) boxes) in a medium-sized office building [12].

Data-driven FDD solutions require a large number of data collected by various measurements in the BAS to perform analytics. A typical data-driven passive FDD process is given in Fig. 1. In the passive FDD process, operation interval data on various measurements of the HVAC system are collected by the BAS, and are fed into FDD approaches to create baseline and calculate residuals. Then, the data-driven FDD approach uses various algorithms to analyze the residual values. An abnormal operation event is flagged when fault symptoms (i.e., the residual calculated from the incoming data and the baseline is higher than the defined threshold) are captured to indicate a fault occurs. After that, the diagnostic process is carried out to identify fault signatures, e.g., the unique fault symptoms on specific measurements that are associated with the specific fault. Through this way, the faulty component location, component type or fault type can be determined. Furthermore, the application and deployment of digital twin technologies require the measurements from the BAS to provide enough information to better indicate the system's operations under both fault-free and faulty conditions [16].

The sensitivity of a measurement indicates how the operation interval data collected by measurements may contain necessary information associated with a fault (i.e., representing fault signatures). In the BAS, not all measurements are sensitive to faults, and hence the data collected by those measurements contain little information to identify fault signatures.

In the past, a few studies performed measurement sensitivity analyses under the system's faulty operation to validate fault models, develop rule-based FDD approaches, and optimize sensor locations. For example, Rossi et al. evaluated the measurement sensitivity for vapor compression air conditioners [17]. In the study, fault symptoms on seven temperature measurements and one humidity measurement to extract generic rules under five types of faults. Furthermore, the authors demonstrated that the developed FDD approach was sensitive to various measurements and had different diagnostic capabilities. However, the study only provided the symptom directions on each measurement and did not quantify the measurement sensitivity. Breuker et al. investigated fault impacts on seven temperature measurements in rooftop air conditioners [18]. In the study, 96 transient tests were performed at four load levels and 24 fault severity levels for five common faults in rooftop air conditioners to evaluate both transient and steady effects on the

measurements. The temperature changing directions under different faults were summarized to form generic rules which can be used to develop FDD tools. Similarly, the research did not quantify the measurement sensitivity. McIntosh et al. analyzed the sensitive characteristic quantities (CQs) of 11 measurements when developing the FDD approach for chillers [19]. In the study, the sensitive CQs include the value change directions and relative magnitudes on each measurement when the chiller operates under a type of fault or operates under two normal operating conditions (i.e., load change and heat rejection change). For six fault types in chillers, different sensitive CQs were proposed for fault identification. Comstock et al. proposed a new metric, namely the sensitivity ratio, to quantify the steady-state measurement sensitivity under eight common faults in chillers [20]. The sensitivity ratio was calculated by comparing the residual of a given measurement at the highest severe level and the maximum experimental uncertainty of the given measurement. The authors investigated measurement sensitivities under various chiller load conditions and fault severity levels. Chen et al. studied fault impacts on eight measurements when developing simple rule-based methods for packaged air conditioners [21]. In addition to using the sensitivity ratio which was developed in Ref. [21], Chen and Braun also showed the deviation degree of each measurement under equipment's faulty operation by using simple symbol labels. The authors found that many measurements on packaged air conditioners were actually insensitive to the faults, especially when faults were less severe. With the obtained measurement sensitivity results, the authors identified various measurements which could be used to diagnose faults with the severity thresholds. Similarly, when developing a rule-based reasoning method to diagnose faults in typical centrifugal chillers. Xiao et al. integrated the analysis of the measurement sensitivity to enhance the diagnostics accuracy [22]. In the study, both the sensitivity and the relative sensitivity of a measurement were defined by comparing the residual of a measurement and the predefined threshold. Cho et al. employed a transient pattern analysis to investigate fault symptom patterns on measurements in the VAV system [23]. In the study, the time evolution of fault patterns on various measurements were classified into fast and slow patterns based on the lab experimental tests. They found that incorrect fault diagnostics could be generated if the time patterns were not considered in the FDD analysis. Shi et al. used z-score to quantify fault symptom intensities on measurements to assess the fault impacts [24]. The authors simulated four faults in an AHU or in building envelopes at different fault intensities.

In addition to experiment-based measurement sensitivity analyses illustrated above, some FDD approaches employ a feature extraction/selection process, which tries to extract information and select more important features or measurements from system operation [15,25, 26–28].

1.2. Research gaps

Although a handful of studies investigated the measurement sensitivity analysis associated with some HVAC equipment, we identified some research gaps as below.

1) A large body of research employed symbols to qualitatively analyze measurement sensitivities. For example, feature residual may have
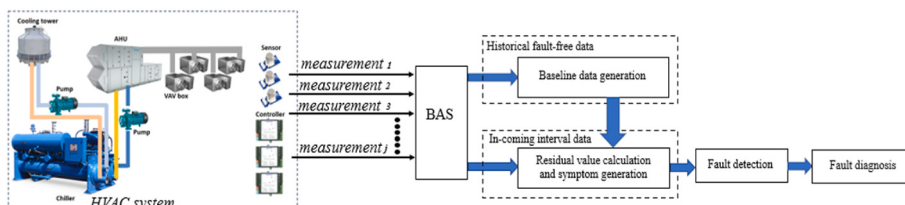

Fig. 1. Common process of passive FDD for HVAC systems.

one of three values; positive or up-arrow (↑), negative or down-arrow (↓), or neutral (i.e., no change, (–)) [18,20,25,29,30]. Similarly, the positive symbol (+) or the negative symbol (−) were used to indicate whether the deviation on a measurement is higher or lower than the baseline [21]. However, very little research quantified the measurement sensitivities. Although using ssymbols to qualitatively can indicate how a fault may cause effects on measurements, those representations neglect the uncertainties caused by fault severities and fault occurrence likelihood. Furthermore, those symbols can hardly be used in any calculations which are needed in various applications.

2) Some research proposed data-driven feature selection approaches to select measurements from HVAC systems [15,25,26–28]. In addition, some studies used Sobol's index [31]. However, the selection process of features (i.e., measurements) and Sobol's method were normally carried out using data collected in the fault free operation. The measurement sensitivity under faulty operations can be very different and can be affected by factors such as fault severity levels and operation conditions. Consequently, those results can be hardly used to completely evaluate the measurement sensitivity to a fault.

3) Several studies evaluated measurement sensitivity of faults on the chiller and vapor compression air conditioner years ago [17,20,22]. However, very little research has been carried out to evaluate the measurement sensitivity in the air distribution subsystem (e.g., the air handling units (AHUs) or variable air volume (VAV) boxes). Therefore, it is necessary to investigate the measurement sensitivity in the air distribution subsystems.

4) Several studies investigated the measurement sensitivity from an individual component (e.g., chillers and packaged rooftop units). However, to the authors' best knowledge, no research has been carried out to study the sensitivities of measurements across different levels, i.e., when a fault occurs in an equipment at the upstream level, whether the measurements in the downstream system are sensitive to the fault. In an HVAC system, measurement sensitivities may be affected by various factors such as system physical configurations, and control sequences [3]. For example, if a cooling coil valve is stuck at a higher than a normal position, the air handling unit (AHU) will provide excessive cooling to zones. This fault not only causes the supply air temperature to be lower, but also may affect the discharge air temperature in the downstream VAV boxes. Therefore, there is a need to analyze how measurements at various levels of the HVAC system are sensitive to a fault.

5) Existing research seldom investigated the measurement sensitivity to a fault in all operational conditions. Although some research investigated fault impacts under different operational seasons [24,26], the analysis of measurement sensitivities should consider more factors such as building internal loads. This is especially critical for the air distribution system, where the measurement sensitivity is highly affected by various operation statuses due to varied internal loads.

Therefore, a complete investigation of measurement sensitivity under various faults is essential to develop various FDD solutions, evaluate fault detectability and diagnosability, as well as efficiently deploy sensors and collect data.

1.3. Contributions

In this study, we proposed a fault symptom-driven method to evaluate measurement sensitivity under common faults in a HVAC system. Because fault symptoms (i.e., the deviation of measured value under a faulty operation from the baseline value) on each measurement are the direct indications of a fault, the occurrence of a fault symptom can be used to evaluate the measurement sensitivity. We calculated fault symptom occurrence probability (SOP) of each measurement and performed statistical pattern analysis to evaluate the measurement sensitivity. In addition, we developed sensitivity indices to quantify the measurement sensitivity patterns under common HVAC system faults.

To fully understand the measurement sensitivity in an air distribution system, we employed fault simulation data of an VAV HVAC system [32]. The HVAC system, which represents a typical air distribution system, includes one dual duct AHU and four associated VAV boxes.

The contribution of this paper has three aspects.

● A novel sensitivity analysis method, which includes two new sensitivity indices, namely the SI of a fault (SI_fault) and the global measurement SI (SI_measurement_global), is proposed to quantify how a measurement is sensitive to a specific type of a fault, or all common faults in the HVAC system. The SIs are calculated by using the symptom occurrence probability distribution, fault occurrence probability distributions and fault severity probability distributions.
● The simulated HVAC system contains 89 measurements in different levels (i.e., the upstream AHU side and downstream VAV side), so that the developed SIs aresystematically evaluated.
● The important measurements, which show strong sensitivities under system faulty operation, can be manifested to identify fault signatures and used for multiple data-driven FDD applications.

The reminder of this paper is organized as: Section 2 illustrates the research methodology. Section 3 presents the fault simulation. Section 4 illustrates the analysis of the sensitivity indices, as well as provides one case study to demonstrate the usage of the SIs. Section 5 concludes the paper and proposes the future work.

2. Methodology

In this study, we employed the fault symptom-based method to quantify the measurement sensitivity. We provide an overview of the method in Section 2.1. Finally, we detailed the method through Sections 2.2 to 2.5.

2.1. Overview of the method

Fig. 2 illustrates the method framework which includes four elements. First, we explain how fault symptoms can be used to analyze the measurement sensitivity. Secondly, we propose a baseline generation method, named weather and internal thermal load pattern matching-based method. The method was used to accurately generate fault symptoms under different operations of the HVAC system. Thirdly, we illustrate the calculation of the fault symptom occurrence probability (SOP). Lastly, we demonstrate the calculation process of the measurement SIs.

2.2. Fault symptom-based measurement sensitivity analysis

In an HVAC system, a fault can cause deviations of measured values on various measurements from the baseline [33]. The deviations on the measurement can be considered as fault symptoms. A larger magnitude of the deviation indicates a strong fault symptom, which is more likely to be observed. On the contrary, if the magnitude of the deviation is too small, the fault symptoms are weak and may not be easily captured. If a measurement is more sensitive to a fault, it means that the fault can cause significant deviations from the baseline on the measurement, i.e., fault symptoms can be easily captured by the measurements. Therefore, observing the occurrence of fault symptoms on a specific measurement when a fault occurs can efficiently assess how the measurement is sensitive to the fault.

In [34], Chen et al. illustrated three approaches to identify fault symptoms on various measurements when a fault occurs. In addition, Chen et al. proposed using symptom occurrence probability (SOP) to quantify fault effects with uncertainties [34]. Considering the fault effects evaluation facilitates the analysis of measurement sensitivities, we adopted the same analysis scenario in this study. Therefore, we first analyzed fault symptom patterns.
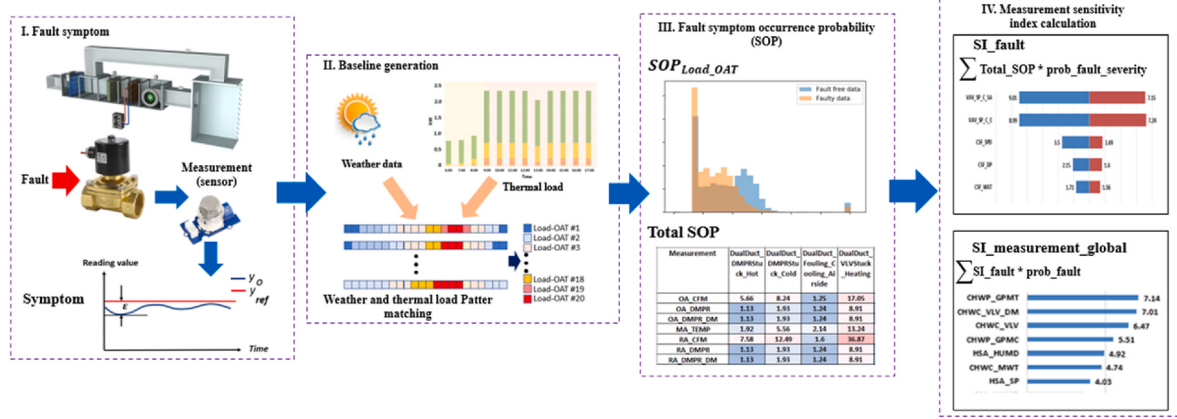
Fig. 2. Overview of the method.

To generate fault symptoms, we compared the snapshot fault data and the normalized baseline data on each measurement to indicate an observable fault symptom. The normalized baseline data are generated through each binned load and outdoor air temperature (Load-OAT) window as will be illustrated in Section 2.3. Within each binned Load-OAT window, the mean value and the standard deviation of the operation data on each measurement can be calculated using Eq (1).

$$
\left\{
\begin{array}{l}
\mu = \dfrac{1}{n} \sum_{i=1}^{n} y_i \\[2ex]
\sigma = \sqrt{\dfrac{1}{n-1} \sum_{i=1}^{n} (y_i - \mu)^2}
\end{array}
\right\}
\qquad \text{Eq 1}
$$

where, y_i is the ith data sample collected by each measurement, n is the total observation, μ is the mean value, and σ is the standard deviation of the measurement.

Therefore, an observable fault symptom can be obtained when the absolute difference between each observation and the mean value of measurement is higher than the standard deviation as given in Eq (2).

$$
|y_i - \mu| > t \times \sigma \qquad \text{Eq 2}
$$

where, t is the threshold value to determine the measurement sensitivity (e.g., 1, 2, …). In this study, t is set to three as the threshold (with a 99.7% confidence level when assuming the distributions of deviations on each measurement to be normal distributed). Therefore, a lower threshold may increase the sensitivity of a measurement considering some HVAC system faults (especially at a minor severity level) may not generate significant measured deviations (i.e., symptoms) on measurements.

It is noted that in an HVAC system, the fault symptom direction (i.e., the deviation direction compared with the baseline data) can be different for the same type fault under different operating conditions. For instance, if an outdoor air damper is stuck at a higher position in an AHU, the mixed air temperature could be higher than the baseline when the OAT is high (e.g., in the summer season), and could be lower than the baseline when the OAT is low (e.g., in the winter season). As a result, a fault diagnosis process also needs to consider the correct identification of fault symptom directions under various operating conditions. Hence, when evaluating the measurement sensitivity, we considered both positive symptoms and negative symptoms.

2.3. Weather and internal thermal load pattern matching-based baseline data generation

The generation of varying baseline data sets, which accurately match the system's various operational patterns, is critical to producing fault symptoms [35]. In an HVAC system's operation, two factors may significantly affect the system operating patterns [15,36]. One factor is the internal load which comes from either occupants or various types of equipment (e.g., lighting and plug-in appliances) in buildings. The HVAC system needs to be operated to provide required cooling for internal heat gains. Another factor is the weather conditions (e.g., temperature and solar radiant), which can cause heat gain or heat loss to buildings; and consequently, affect HVAC system operations. Additionally, weather information is used in control sequences in some types of equipment to automatically adjust the operating modes and execute control logics. For example, the AHU economizer operating mode can be controlled by comparing the OAT and mixed air temperature.

Although some literature used different operating seasons (i.e., winter seasons, summer seasons and shoulder seasons) to group operational data to generate the baseline, and analyze the fault impacts with each operating season [37], the baseline data subsets generated on three operating seasons may not accurately reflect the system's operating patterns and fault effects on various measurements. This is because the current HVAC system's operation is seldom controlled according to the strict seasonal classifications. Although some chiller plants' operation can be manually switched in different seasons (i.e., turn on chillers in shoulder seasons and turn off chillers in winter seasons), more and more HVAC systems, especially secondary air distribution systems, including AHUs, are automatically controlled according to weather and internal load conditions instead of being controlled based on the predefined operating seasons. As a result, the system's operating patterns can be different even within one operating season; and hence the baseline data cannot be generated by simply grouping fault free data within the same operating season.

To address this issue, some studies developed HVAC system operating pattern matching approaches [15,38]. For example, a weather and schedule-based operating pattern match strategy was developed to map incoming operating data of an HVAC system with the historical baseline data so that similar operating patterns can be matched for system level fault diagnostics [15].

In this study, we developed a weather and internal thermal load pattern matching-based method which employed both real time weather information and building load information to generate the baseline data. This method is divided into two steps. First, the internal thermal load patterns are determined to group operating periods during occupied hours on weekdays. Secondly, the operating periods within each internal load pattern is further grouped according to the similar weather information. In this study, we used the outdoor air temperature (OAT) as the indicator to match operating patterns because 1) OAT is a major factor to affect the HVAC system's operation [39]; and 2) in the VAV HVAC system in this study, some dual duct AHU control sequences are determined by the OAT. For example, when OAT is higher than 15.6 °C, the

AHU is switched to operate in the mechanical cooling mode. Under such an operating mode, the cooling coil valve position is adjusted from 0% to 100%, and the outdoor air damper is operated at the minimum open position (e.g., 15%–20% opening position).

The internal zone load settings are the same for all four separate zones as illustrated in Section 3.2. Hence, the internal thermal load can be determined by considering the aggregated load from all four zones. Load settings were grouped according to their magnitude range. In this study, we used two load levels as 1) the load level #1 as the zone internal load is equal or lower than 1.0 kW, and 2) the load level #2 as the zone internal load is higher than 2.0 kW. This is based on the load settings in the simulation as indicated in Fig. 5.

Then, within each internal thermal load level, the OAT is equally binned into equal sized windows. The number of windows is determined by the consideration of two factors as 1) the system operational pattern within each binned OAT window should be similar; and 2) the sample size within each binned OAT window is sufficient. In this study, the OAT in each load level is equally binned into ten windows, resulting in a bin size of 4.80 °C for the load level #1 and 5.15 °C for the load level #2.

In this study, the simulation output rate was set to 1-min time interval. Consequently, for the fault-free test case and each fault test case, the simulation generates a total of 187,920 operating minutes (i.e., the number of samples under a 1-min sampling rate and 12 operating hours

the total SOP of a measurement under each specific fault case (i.e., one fault with one severity level). First, under each data subset of the operation status, the SOP can be calculated by counting the frequency of the symptom observations on each measurement under a specific fault type and a fault level as given in Eq (3).

$$Prob\left(fault\_sym|OP_{Load\_OAT}\right) = \frac{\sum num\_fault\_sym}{OP\_Duration\_Load\_OAT} \qquad Eq\ 3$$

where $Prob\left(fault\_sym|OP_{Load\_OAT}\right)$ is the SOP value under each binned Load-OAT window for one type of a fault under one severity level. $\sum num\_fault\_sym$ is the total number of fault symptoms observed. Because two fault symptom directions can be calculated respectively, $Prob\left(fault\_sym|OP_{Load\_OAT}\right)$ can be calculated for positive symptoms and negative symptoms, respectively. $OP\_Duration\_Load\_OAT$ is the length of each Load-OAT window.

Secondly, the total SOP (Prob (fault_sym_total)) can be calculated by using the law of total probability (can also be interpreted as a weighted average) in the Bayesian approach. For each measurement, the SOP values (i.e., $Prob\left(fault\_sym|OP_{Load\_OAT}\right)$) obtained in each Load-OAT window can be aggregated to obtain the total SOP distributions as given in Eq (4).

$$Prob(fault\_sym\_total) = \sum_{i}^{num\_bin\_window} Prob\left(fault\_sym|OP_{Load-OAT}\right)_i Prob\left(OP_{Load-OAT}\right)_i \qquad Eq\ 4$$

each day) from 261 operating days for each test case in one year.

As ten binned OAT windows were used for each internal thermal load level, 20 Load-OAT windows (i.e., ten OAT ranges in each load level) were generated. For load level #1 (i.e., internal load below 2.0 kW), a 3-h operating duration each day (i.e., from 6:00 to 8:59) is obtained, resulting in 46,980 min of a year. For load level #2, (i.e., internal load level is above 2.0 kW), the operation duration is 9 h each day (i.e., from 9:00 to 17:59), resulting in a total of 140,940 min of a year.

Table 1 (a) and (b) list the median OAT value, operation duration (i. e., sample size) and operation duration ratio within each Load-OAT window for load level #1 and #2, respectively. For each Load-OAT window, the operation duration ratio is calculated by dividing the operation duration (minutes) by the total operating minutes (i.e., 187,920 min). For example, for L1-bin #1, the operation duration ratio (0.88%) is calculated by dividing 1662 by 187,920.

2.4. Calculation of fault symptom occurrence probability

In this study, we used the symptom occurrence probability (SOP) metric, which was originally developed to evaluate fan coil unit fault effects [34], to evaluate the measurement sensitivity under each fault type and with different fault severity levels. The fault severity level is the magnitude of a fault. For a hardware related fault, it can be related to the physical size of a fault. For example, a sensor bias fault at 2 °F indicates a 2 °F deviation of the sensor reading from the real value. For software related faults, it can be the magnitude of the parameter setting deviated from the normal setting. In Ref. [34], two steps were used to calculate

where $Prob(OP_{Load-OAT})_i$ is the operation duration ratio of the ith binned Load_OAT window. Table 1 lists the operation duration and the operation duration ratio within each binned Load_OAT window. Num_bin_window is the total number of binned Load_OAT windows. In this study, the num_bin_window is set to 20 because 20 Load-OAT windows are used for two load levels together. Therefore, the sum of the operation duration ratio for all 20 binned Load_OAT windows is 100%, indicating all operation conditions.Table 2

2.5. Development of measurement sensitivity indices

The calculation of the measurement SI of a fault (SI_fault) and the global measurement SI (SI_measurement_global) incorporated the fault severity probability distribution and the fault occurrence probability, respectively.

For each type of fault, a fault occurrence probability is the occurrence likelihood of a fault. The fault occurrence probability can be measured in multiple ways. For example, the probability distribution can be obtained by measuring how often a specific type of a fault occurs within a certain period of time [40]. For each type of a fault, a fault severity probability is the likelihood of a fault occurrence at a certain severity level. Table 3 lists the fault severity probability and the fault occurrence probability for each type of fault. In this study, the fault severity levels we selected are based on two considerations. First the fault severity levels we used are commonly reported in the previous FDD literature. Hence, we thought they should represent the common understanding of HVAC system faults in the research area. Secondly, the

Table 1 (a)
Operation duration and time ratio under internal load level 1 (L1).

Bin No.	L1-bin #1	L1-bin #2	L1-bin #3	L1-bin #4	L1-bin #5	L1-bin #6	L1-bin #7	L1-bin #8	L1-bin #9	L1-bin #10
Median OAT (°C)	−20.64	−15.32	−9.98	−4.66	0.67	5.99	11.32	16.65	21.98	27.31
Operation duration (minutes)	1662	2119	2599	4257	8327	5587	4743	6631	9046	2009
Duration ratio (%)	0.88	1.13	1.38	2.27	4.43	2.97	2.52	3.53	4.81	1.07

Table 1 (B)
Operation duration and time ratio under internal load level 2 (L2).

Bin No.	L2-bin #1	L2-bin #2	L2-bin #3	L2-bin #4	L2-bin #5	L2-bin #6	L2-bin #7	L2-bin #8	L2-bin #9	L2-bin #10
Median OAT (°C)	−18.25	−12.53	−6.81	−1.09	4.63	10.36	16.08	21.80	27.52	33.24
Operation duration (minutes)	1590	6303	8788	16,339	18,946	15,897	14,239	22,673	28,388	7777
Duration ratio (%)	0.85	3.35	4.68	8.69	10.08	8.46	7.58	12.07	15.11	4.14

primary purpose of this study is to illustrate the novel method, which can effectively evaluate measurement sensitivities. Therefore, using this method, the measurement sensitivities under common faults can be better quantified if more fault severity levels and associated occurrence probabilities can be added into the index calculation. It is noted that there are no complete fault occurrence probability distributions (for a specific type of a fault, or a fault at various severity levels) reported. Therefore, in this study, we employed expert estimates for the occurrence probability distributions to calculate the SIs. Consequently, the SIs can be adjusted when the occurrence probability distributions are updated.

We incorporated both fault occurrence probability distributions and fault severity probability distributions into the calculation of the measurement SIs for two reasons. First, a measurement is sensitive to a specific type of a fault at different severity levels. For example, the supply air temperature sensor of an AHU is more sensitive to the AHU cooling coil valve stuck fault at a 100% position than the same fault but at a 20% position severity level because the air temperature sensor will generate a higher SOP (i.e., probability of the temperature lower than the baseline), when the cooling valve is stuck at a 100% position than the SOP when the cooling valve is stuck at a 20% position. However, the occurrence likelihood of a fault at a certain severity level is different. Therefore, it will be more accurate to evaluate the sensitivity of a measurement to a specific type of a fault considering the occurrence likelihood of a specific type of a fault at a severity level. Secondly, a measurement is sensitive to different types of faults. When evaluating the overall sensitivity of a measurement under all types of faults, it needs to consider the likelihoods of the occurrence of all possible faults.

2.5.1. Sensitivity index of a fault (SI_fault)

The SI_fault quantifies how a measurement is sensitive to a specific type of fault. In the calculation of the SI_fault, we considered the fault severity. The SI_fault can be calculated given in Eqs (5)–(7). Equations (5) and (6) illustrates the calculation of SI for the positive symptoms and negative symptoms

$$\text{SI\_fault\_positive} = \sum_{k=0}^{n} \left(Prob(fault\_sym\_total)_{pos\_k} \right.$$
$$\left. * \ Prob(fault\_severity)_{pos\_k} \right) \qquad \text{Eq 5}$$

$$\text{SI\_fault\_negative} = \sum_{k=0}^{n} \left(Prob(fault\_sym\_total)_{neg\_k} \right.$$
$$\left. * \ Prob(fault\_severity)_{neg\_k} \right) \qquad \text{Eq 6}$$

where $Prob(fault\_sym\_total)_k$ is the $Prob(fault\_sym\_total)$ of the kth fault case (i.e., one fault type under one severity level) that is calculated from Eq (4). $Prob(fault\_severity)_k$ is the fault severity probability. For each type of fault, the $Prob(fault\_severity)$ value can be found in Table 3.

The aggregated SI_fault (SI_fault_sum) can be calculated by summing *SI_fault_positive* and *SI_fault_negative* together as given by Eq (7).

$$\text{SI\_fault\_sum} = \text{SI\_fault\_positive} + \text{SI\_fault\_negative} \qquad \text{Eq 7}$$

2.5.2. Global measurement sensitivity index (SI_measurement_global)

The SI_measurement_global aggregates the SI_fault (including both positive and negative) calculated from each type of a fault. This index quantifies how a measurement is overly sensitive to all possible faults considered. The SI_measurement_global can be calculated given in Eq (8). The calculation of the SI_measurement_global includes the fault occurrence probability distributions. Consequently, if the fault occurrence probability value is higher for specific types of faults, the SI_measurement_global value of a specific measurement could be higher, indicating that this measurement is more sensitive to the fault. Therefore, the measurement will be considered as a key performance indicator (KPI). The SI_measurement_global can be used to optimize the measurement deployment in the monitoring system.

$$\text{SI\_measurement\_global} = \sum_{j=0}^{n} \left(\text{SI\_fault\_sum}_j * Prob(fault)_j \right) \qquad \text{Eq 8}$$

where $Prob(fault)_j$ is the fault occurrence probability of the jth fault type as illustrated in Table 3.

In the study, we investigated common fault types that are reported in the HVAC system operation. However, the SI_measurement_global value can be updated when more knowledge on HVAC system faults is obtained using the proposed calculation approach.

3. Fault simulation

In this study, we employed simulation data which were generated in HVACSIM+ environment to analyze the measurement sensitivity. The FDD data were curated by Granderson et al. [32]. In this section, we illustrate the system model in Section 3.1. In Section 3.2, we describe the simulation settings. In Section 3.3, we introduce the fault simulation process.

3.1. Simulation platform

3.1.1. Simulation software

In this study, a previously developed VAV HVAC system simulation model was employed to simulate various faults. The VAV HVAC system, including both the dual-duct AHU and four associated VAV boxes, were modeled using the HVACSIM+ simulation software developed by National Institute of Standards and Technology [41].

HVACSIM+ uses a hierarchical structure where individual UNITs, each defined by a specific TYPE template representing a generic system component, are linked together to mimic their real-world interactions. These UNITs are organized into Blocks and Superblocks, allowing for simultaneous solutions and treating each Superblock as an independent subsystem in the overall simulation [41]. In this study, we employed an advanced numerical solver developed in Ref. [42] to efficiently solve the resulting nonlinear algebraic and differential equations within each Superblock. Fig. 3 illustrates the superblock hierarchy of the simulation of the dual duct AHU. The hierarchical modeling process enables the development of a complex system model, which may include multiple levels of equipment in a HVAC system (e.g., five levels shown in the figure). The detailed model development process can be found in Ref. [43].

3.1.2. Simulated HVAC system

The simulation model was developed based on a VAV HVAC system, which was originally installed at the Energy Resource Station (ERS) of the Iowa Energy Center. The VAV HVAC system includes a dual-duct

Table 2

List of measurements.

NO.	Measurement name	Description	Measurement type	Unit
DDAHU side				
1	OA_CFM	Outdoor air flow rate	Sensor	CFM
2	OA_DMPR	Outdoor air damper position signal	Sensor	Open (0–1)
3	OA_DMPR_DM	Outdoor air damper control signal (command)	Control signal	Open (0–1)
4	MA_TEMP	Mixed air temperature	Sensor	°F
5	RA_CFM	Return air flow rate (sum of all zones returns)	Sensor	CFM
6	RA_DMPR	Return air damper position signal	Sensor	Open (0–1)
7	RA_DMPR_DM	Return air damper control signal	Control signal	Open (0–1)
8	RA_HUMD	Return air humidity	Sensor	%RH
9	RA_TEMP	Return air temperature	Sensor	°F
10	RF_DP	Return fan differential pressure	Sensor	in.w.g.
11	RF_SPD	Return fan VFD speed	Sensor	Speed (0–1)
12	RF_WAT	Return fan power	Meter	Watt
13	EA_DMPR	Exhaust air damper position signal	Sensor	Open (0–1)
14	EA_DMPR_DM	Exhaust air damper control signal (command)	Control signal	Open (0–1)
15	HSA_SP	Hot deck supply air duct static pressure	Sensor	in.w.g.
16	HSA_HUMD	Hot deck supply air humidity	Sensor	%RH
17	HSA_CFM	Hot deck supply air flow rate	Sensor	CFM
18	HSA_TEMP	Hot deck supply air temperature	Sensor	°F
19	HSF_DP	Hot deck supply fan differential pressure	Sensor	in.w.g.
20	HSF_SPD	Hot deck supply fan VFD speed	Sensor	Speed (0–1)
21	HSF_WAT	Hot deck supply fan power	Meter	Watt
22	CSA_SP	Cold deck supply air duct static pressure	Sensor	in.w.g.
23	CSA_HUMD	Cold deck supply air humidity	Sensor	%RH
24	CSA_CFM	Cold deck supply air flow rate	Sensor	CFM
25	CSA_TEMP	Cold deck supply air temperature	Sensor	°F
26	CSF_DP	Cold deck supply fan differential pressure	Sensor	in.w.g.
27	CSF_SPD	Cold deck supply fan VFD speed	Sensor	Speed (0–1)
28	CSF_WAT	Cold deck supply fan power	Meter	Watt
29	HWC_DAT	Heating water coil discharge air temperature	Sensor	°F
30	HWC_EWT	Heating water coil entering water temperature	Sensor	°F
31	HWC_LWT	Heating water coil leaving water temperature	Sensor	°F
32	HWC_MWT	Heating water coil mixed water temperature	Sensor	°F
33	HWC_VLV	Heating water coil valve position signal	Sensor	Open (0–1)
34	HWC_VLV_DM	Heating water coil valve control signal	Control signal	Open (0–1)

Table 2 (*continued*)

NO.	Measurement name	Description	Measurement type	Unit
35	HWP_GPMC	Heating water pump water flow rate through coil	Sensor	GPM
36	HWP_GPMT	Heating water pump total water flow rate	Sensor	GPM
37	CHWC_DAT	Cooling coil discharge air temperature	Sensor	°F
38	CHWC_EAH	Cooling coil entering air relative humidity	Sensor	%RH
39	CHWC_EWT	Cooling coil entering water temperature	Sensor	°F
40	CHWC_LWT	Cooling coil leaving water temperature	Sensor	°F
41	CHWC_MWT	Cooling coil mixed water temperature	Sensor	°F
42	CHWC_VLV	Cooling coil valve position signal	Sensor	Open (0–1)
43	CHWC_VLV_DM	Cooling coil valve control signal	Control signal	Open (0–1)
44	CHWP_GPMC	Chilled water pump water flow rate through coil	Sensor	GPM
45	CHWP_GPMT	Chilled water pump total water flow rate	Sensor	GPM
VAV box side (Measurement names followed by _W, _SB, _SA, _and E, respectively to indicate different VAV boxes)				
1	RM_TEMP	Room temperature	Sensor	°F
2	VAV_DAT	Mixing box discharge air temperature	Sensor	°F
3	VAV_SP_C	Mixing box cold deck dynamic pressure	Sensor	in.w.g.
4	VAV_SP_H	Mixing box hot deck dynamic pressure	Sensor	in.w.g.
5	VAV_DMPR_C	Mixing box cold deck damper control signal	Control signal	Open (0–1)
6	VAV_DMPR_H	Mixing box hot deck damper control signal	Control signal	Open (0–1)
7	VAVCFM_C	Mixing box cold deck air flow rate	Sensor	CFM
8	VAVCFM_H	Mixing box hot deck air flow rate	Sensor	CFM
9	VAVCFM_T	Mixing box total air flow rate	Sensor	CFM
10	VAV_EAT_C	Mixing box cold deck entering air temperature	Sensor	°F
11	VAV_EAT_H	Mixing box hot deck entering air temperature	Sensor	°F

AHU and four associated VAV boxes in four zones as shown in Fig. 4. The dual duct AHU system equips two separate supply air ducts as hot duct and cold duct, and two supply air fans in each duct to provide desired air circulation and thermal comfort to different zones. In this system, both the heating and cooling coils can operate at the same time. The hot air and the cold air will be mixed with dampers in VAV boxes at each zone. Four VAV boxes are installed in four rooms (i.e., East, South A, South B and West) at the ERS.

Fig. 5 illustrates the detailed deployment location of each measurement. In the schematic, we demonstrate measurements in the AHU and one associated VAV box. The measurement deployment in the other three VAV boxes is the same with the VAV box shown in this schematic. Furthermore, we illustrate the location where the fault was injected.

3.1.3. Description of measurements

Data collected from various measurements in the BAS are employed by various data-driven FDD solutions. The measurement can be categorized into three types as sensor readings, control command signals, and meter readings. In Fig. 4, various measurements are color-labeled such that the red color texts represent sensor readings, the blue color

Table 3
Fault information.

Fault ID/Fault name	Fault severity level	Fault occurrence probability	Fault severity probability	Fault ID/Fault name	Fault severity level	Fault occurrence probability	Fault severity probability
F1: SensorBias_CSA	+2 °C	0.1	0.1	**F7:** DMPRStuck_Cold	Stuck at 0%	0.05	0.1
	+4 °C		0.1		Stuck at 100%		0.1
	−2 °C		0.1		Stuck at 20%		0.25
	−4 °C		0.1		Stuck at 50%		0.2
F2:	+2 °C	0.1	0.1		Stuck at 80%		0.1
SensorBias_HSA	+4 °C		0.1	**F8:** DMPRStuck_Hot	Stuck at 0%	0.05	0.1
	−2 °C		0.1		Stuck at 100%		0.1
	−4 °C		0.1		Stuck at 20%		0.25
F3: SensorBias_CSP	+2 inwg	0.1	0.1		Stuck at 50%		0.2
	+4 inwg		0.1		Stuck at 80%		0.1
	−2 inwg		0.1	**F9:** DMPRStuck_OA	Stuck at 0%	0.05	0.1
	−4 inwg		0.1		Stuck at 100%		0.1
F4: SensorBias_HSP	+2 inwg	0.1	0.1		Stuck at 28%		0.25
	+4 inwg		0.1		Stuck at 45%		0.2
	−2 inwg		0.1		Stuck at 80%		0.1
	−4 inwg		0.1	**F10:** Fouling_Cooling_Waterside	Minor	0.01	0.3
F5: VLVStuck_Cooling	Stuck at 0%	0.05	0.1		Moderate		0.3
	Stuck at 100%		0.1		Severe		0.3
	Stuck at 20%		0.25	**F11:** Fouling_Heating_Waterside	Minor	0.01	0.3
	Stuck at 50%		0.2		Moderate		0.3
	Stuck at 80%		0.1		Severe		0.3
F6: VLVStuck_Heating	Stuck at 0%	0.05	0.1	**F12:** Fouling_Cooling_Airside	Minor	0.02	0.3
	Stuck at 100%		0.1		Moderate		0.3
	Stuck at 20%		0.25		Severe		0.3
	Stuck at 50%		0.2	**F13:**	Minor	0.02	0.3
	Stuck at 80%		0.1	Fouling_Heating_Airside	Moderate		0.3
F14: CoolSeqUnstable	NA	0.3	1		Severe		0.3
				F15: HeatSeqUnstable	NA	0.3	1
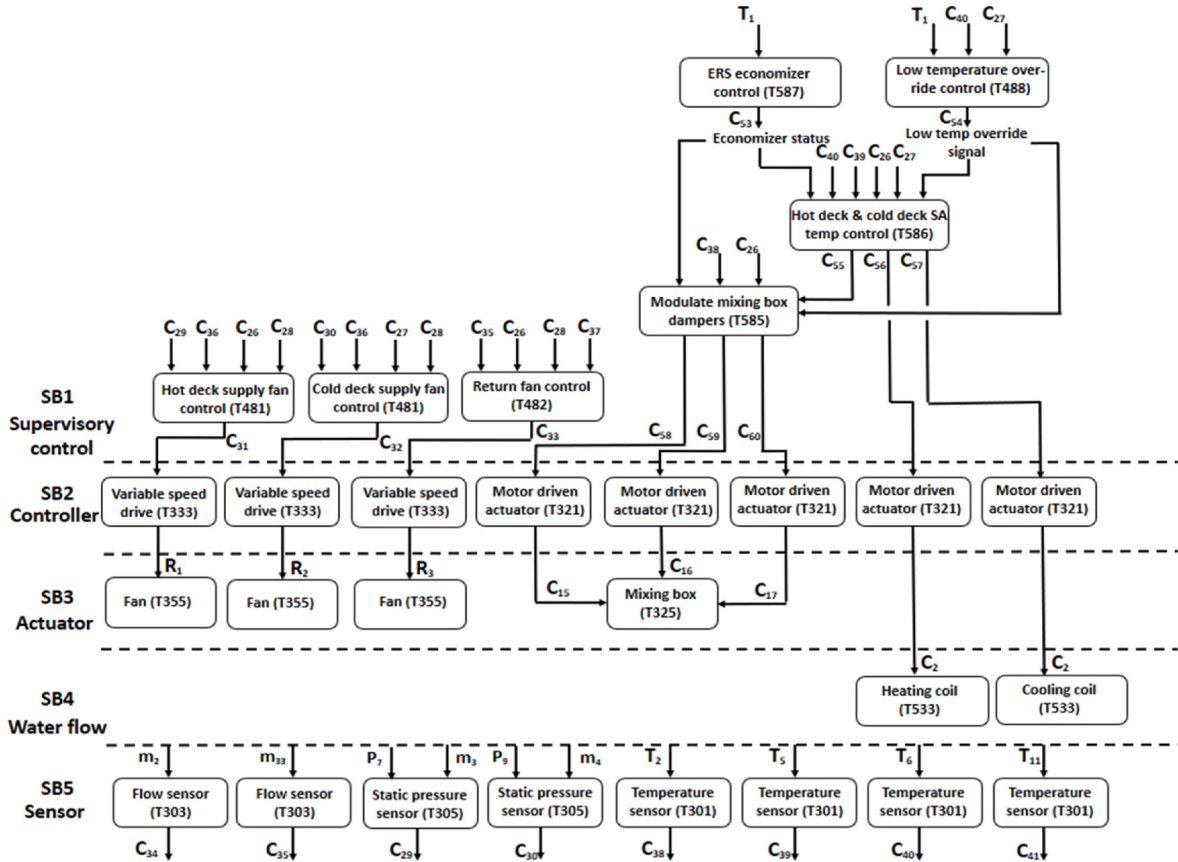
Fig. 3. Example demonstration of the simulation hierarchy.
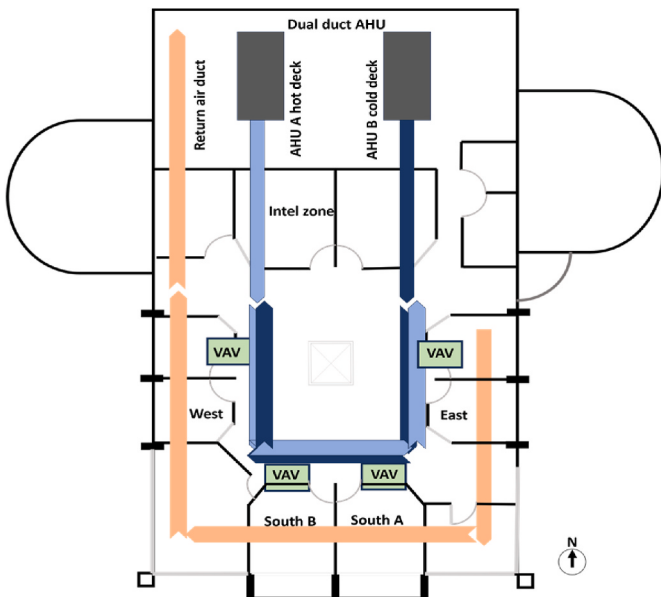
Fig. 4. System configuration at the ERS.

texts represent control signals and the purple color texts represent meter readings, respectively. In the developed simulation model, a total of 89 measurements were used to monitor system operation. Those measurements not only include the measurements in the dual duct AHU, but also include the measurements in downstream VAV boxes because fault effects may propagate to different levels in an HVAC system due to close coupling among various equipment [15]. Table 2 lists the detailed

description of each measurement in the systems. On the AHU side, there are 45 measurements. Among those measurements, 37 measurements collect sensor readings, five measurements collect control signals, and three measurements collect meter data. In each VAV box, nine measurements are sensor readings and two measurements are control signals. It is noted that some measurements may not be often deployed in real practice due to the deployment costs. For example, heating coil discharge air temperature (HWC_DAT) and cooling coil discharge air temperature (CHWC_DAT) were seldom installed in the real system to monitor the system operation performance. But in this study, we also evaluated the sensitivity of those measurements to show that some measurements can be considered in the future design of the BAS to enhance the FDD capabilities.

3.2. Simulation settings

The simulation setting includes three parts as 1) control sequence and parameter settings, 2) zone load settings, and 3) environment parameter settings. The control sequence and parameter settings include setting the operation mode sequence, and individual component control sequences for fan, dampers, cooling coil valve and heating coil valve. Control parameters settings include the settings of proportional and integral gain for the controllers. In terms of zone loads, hourly loads from occupants, lighting and equipment, were determined according to Ref. [43], as shown in Fig. 6. Each zone used the same load setting. The TMY3 weather data for Des Moines, IA was used as the weather inputs because the system model was developed in Iowa in the U.S.

Additionally, the simulation time step was set to 5 seconds. The data sampling rate was set to 1 minute.
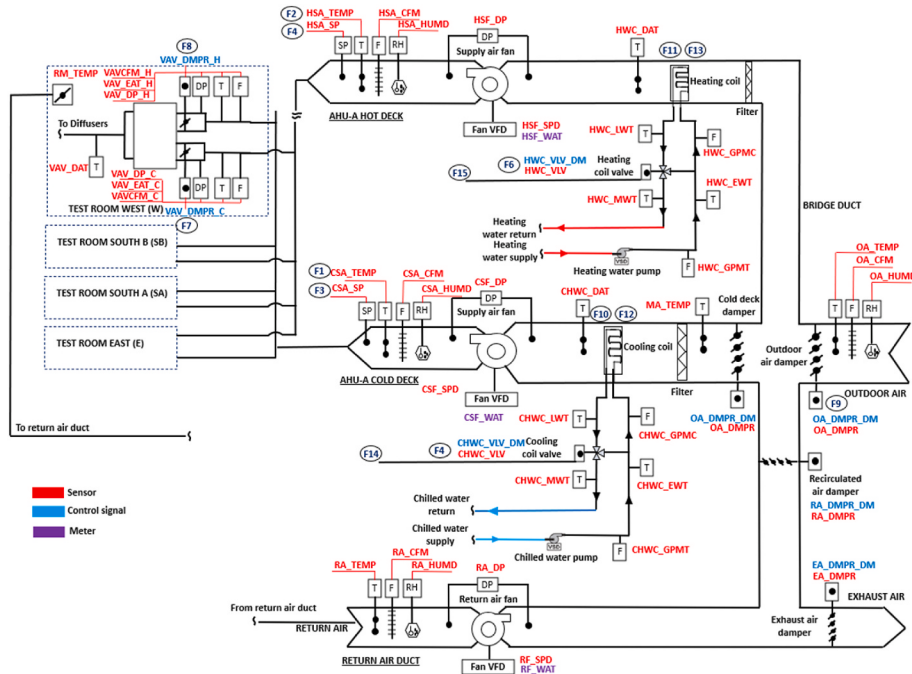
Fig. 5. VAV HVAC system configuration and measurement schematic.
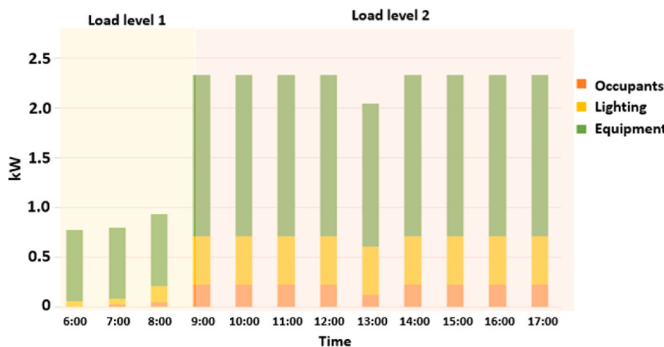
Fig. 6. Hourly zone load setting in the occupied period.

3.3. Simulated faults

In this study, a total of 15 faults which are commonly studied by academic publications and reported by field engineers in the AHU side were imposed to obtain fault inclusive operation data [44–49]. The faults cover hardware faults (i.e., four sensor related faults (F1 to F4), five actuator related faults (F5 to F9), and four stationery component related faults (F10 to F13)) and software setting faults (i.e., two control parameter setting faults (F14 to F15)) as given in Table 3.

For hardware faults, the simulation with multiple severity levels was performed for each type of the fault. For the software faults, the simulation with a single severity level was performed for each type of the fault. Consequently, a total of 55 fault simulation cases were carried out in this study. Each fault case was simulated to generate one year of operation data so that all system's operational conditions can be covered to fully evaluate the measurement sensitivity under various operational conditions.

Each fault simulation case (i.e., one type of a fault at one severity level for one year simulation) was continuously implemented in every operation day (i.e., from 12:00 a.m. to 11:59 p.m.) to obtain a steady operation status. The simulation was performed on a 3.7G CPU, 16 G RAM laptop and the simulation running duration was approximately 8 hours.

Sections 3.3.1 to 3.3.4 detail the description and implementation method for each type of a fault.

3.3.1. Sensor related faults

In an HVAC system, a large number of sensors are deployed to control and monitor the system's operation. Sensor related faults can directly affect control performances because the error signal will be input into the controller, causing improper control output [50].

In this study, we implemented four sensor related faults, which include the supply air temperature sensor bias fault (F1: SensorBias_CSA in the cold duct, and F2: SensorBias_HSA in the hot duct), and the supply air pressure sensor bias fault in both the cold duct and the hot duct (F3: SensorBias_CSP in the cold duct, and F4: SensorBias_HSP in the hot duct). For the sensor bias fault, both bias directions (i.e., the positive bias fault and the negative bias fault) were simulated. For the supply air temperature sensor bias faults, two severity levels (i.e., bias at 2 °C and at 4 °C) in each bias direction were implemented. For the supply air pressure sensor bias faults, two severity levels (i.e., bias at 0.007 psi (0.2 in. wg) and at 0.014 psi (0.4 in. wg)) in each bias direction were implemented. Each bias fault was implemented by adding corresponding value to the sensor output in the TYPE components in the simulation platform. For supply air temperature sensor bias faults in both the cold duct and the hot duct, faulty signals were injected by modifying cold duct and hot duct temperature sensors built in TYPE 311, respectively. For supply air pressure sensor bias faults in both the cold duct and the hot duct, faulty signals were injected by modifying parameters in the pressure sensor model built in TYPE 305, respectively.

3.3.2. Actuator related faults

Various actuators such as dampers, valves and pumps are used to fulfill the control process and enable the system to meet the control objectives. The actuator faults can quickly cause operation performance degradations and hence result in undesired indoor thermal comforts or significant energy wastes. For example, studies show that dampers not working properly faults may cause 5.2 billion kWh/year electricity waste in the U.S [45,51].

In this study, we implemented five actuator related faults, including the cooling valve stuck fault (F5: VLVStuck_Cooling), the heating coil

valve stuck fault (F6: VLVStuck_Heating): the cooling damper stuck fault (F7: DMPRStuck_Cold), the heating damper stuck fault (F8: DMPRStuck_Hot), and the outdoor air damper stuck fault (F9: DMPRStuck_OA). The stuck faults for the cooling coil, the heating coil, and the dampers were simulated at five severity levels as shown in Table 3. The valve stuck faults in the cooling coil and heating coil were injected by assigning a fixed valve position to the output of cooling coil and heating coil components built in TYPE 533. The cooling and heating dampers stuck faults were injected by assigning a fixed damper position to the output of the mixing box component built by either TYPE 531, 532, or 534. Similarly, the outdoor air damper stuck fault was imposed by assigning a fixed damper position to the output of the mixing box component built in TYPE 325.

3.3.3. Stationary component related faults

An HVAC system contains many stationary components such as coils, ducts and filters to supply cooling or heating. Faults in stationary components can cause degradations because the original system design may be violated; and hence lead to cumulative zone thermal comfort deterioration and increased energy consumption. For example, Chen et al. reported that the filter restriction fault can cause 4%–31% annual fan power consumption increase in fan coil units [3]. However, compared to actuator related faults, stationary component related faults are often hardly to be detected because the incipient fault effects may be very small and cannot be easily captured by the FDD tool.

In this study, we implemented four stationary component related faults, which include the cooling coil fouling water-side fault (F10: Fouling_Cooling_Waterside), and the heating coil fouling water-side fault (F11: Fouling_Heating_Waterside), the cooling coil fouling air-side fault (F12: Fouling_Cooling_Airside), and the heating coil fouling air-side fault (F13: Fouling_Heating_Airside). The coil water-side fouling fault is mainly caused by the deposition of mineral material of circulating water on the surfaces of heat exchanger in contact with water. The coil air-side fouling fault is the decreasing heat transfer capability and is mainly caused by the increased heat resistance such as dust on the coil plate fin.

For the Fouling_Heating_Waterside and Fouling_Cooling_Waterside faults, three fault severity levels were imposed by decreasing the water flow rate and the decreasing heat transfer rate as shown in Table 3. For the Fouling_Heating_Airside and Fouling_Cooling_Airside faults, three fault severity levels were imposed by increasing airflow resistance and decreasing heat transfer rate as shown in Table 3.

The waterside fouling faults were injected by modifying fin heat transfer coefficient, tube heat transfer coefficient, and the coil fluid flow resistance in the coil components built in TYPE 533. The airside fouling faults were injected by modifying fin and tube heat transfer coefficients in the coil component built by TYPE 533 and the air flow resistance in the flow resistance component built in TYPE 343.

3.3.4. Control software setting faults

Wrong settings of control software (e.g., control parameters or control sequences) can cause the malfunction of controllers, and hence lead to an abnormal operation of a system. For example, studies show that improper control setup and commissioning and software programming errors could cause 3.3 billion kWh/year electricity waste in the U.S [45, 51]. In HVAC systems, common faults in control parameter settings are improper settings of PID parameters in the controllers [52].

In this study, we implemented two control parameter setting related faults, which include the cooling sequence unstable (F14: CoolSeqUnstable) fault, and the heating sequence unstable (F15: HeatSeqUnstable) as given in Table 3. Both faults were imposed by changing the absolute value of the proportional band of the cooling and heating control sequences from a properly tuned value 45.7 to an improper value of 4 in the dual duct supply air temperature control component (TYPE 586), respectively. The poorly tuned PID parameters further result in unstable cooling coil valve and heating coil valve operations,

respectively, and hence oscillating supply air temperatures. For both faults, only one severity level (i.e., only one error proportional band value) was imposed.

4. Results and discussion

In this Section, we illustrate the analysis of the SI_fault (Section 4.1), and the analysis of the SI_measurement_global (Section 4.2). In addition, we discuss two considerations when using the proposed SIs (Section 4.3). Lastly, we also provide one use case of the developed SIs (Section 4.4).

4.1. Analysis of the SI_fault

Here, we use the VLVStuck_Heating fault, the SensorBias_CSP fault, and the CoolSeqUnstable to demonstrate the analysis of the SI_fault result. The complete SI_fault distribution table can be found in Appendix I of the paper.

(1) F3: SensorBias_CSP fault case

The SensorBias_CSP fault is the supply air pressure sensor bias fault in the cold duct as described in Section 3.3.1. Fig. 7 illustrates the positive SI_fault and negative SI_fault, which the values are higher than 1, from all 89 measurements. It can be seen that for this type of the fault, eight measurements present relatively high sensitivity. Among them, the static pressure sensors in four associated VAV boxes rank very high as the SI_fault_negative values are from 8.99 to 9.27, and the SI_fault_positive values are from 7.15 to 7.24. On the AHU side, the cold deck supply air fan speed measurement presents a relatively higher sensitivity because the SI_fault_negative and the SI_fault_positive are 3.5 and 1.69, respectively. We will use the SI_fault_sum (i.e., sum of SI_fault_positive and SI_fault_negative) to analyze fault signatures in Section 4.4.

(2) F6: VLVStuck_Heating fault case

The VLVStuck_Heating fault is the heating coil valve stuck fault as described in Section 3.3.2. Fig. 8 (a) and (b) illustrate the measurements, in which the positive SI_fault or negative SI_fault are higher than 5 from the measurements on the AHU side and the measurements on the VAV box side, respectively.

It can be seen that most measurements are very sensitive to this type of the fault. For example, from the AHU side, the highest SI_fault_negative is 33.79 on the HWC_MWT measurement, indicating that the heating coil mixing water temperature sensor can easily collect negative symptoms (e.g., temperature is lower than the baseline value), when the fault occurs. The measurements of HSA_TEMP, HWC_DAT, and HWC_LWT are the top three sensitive measurements based on the
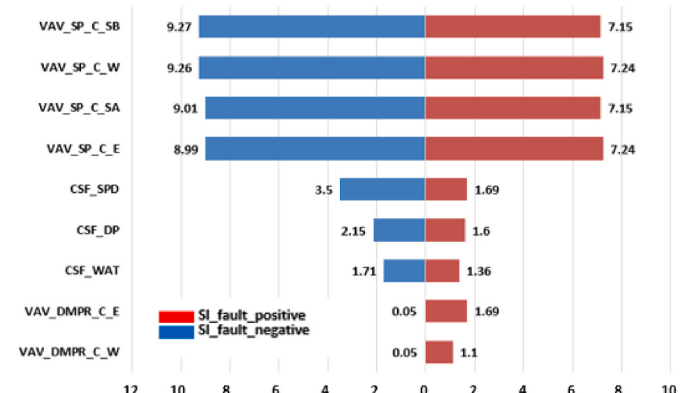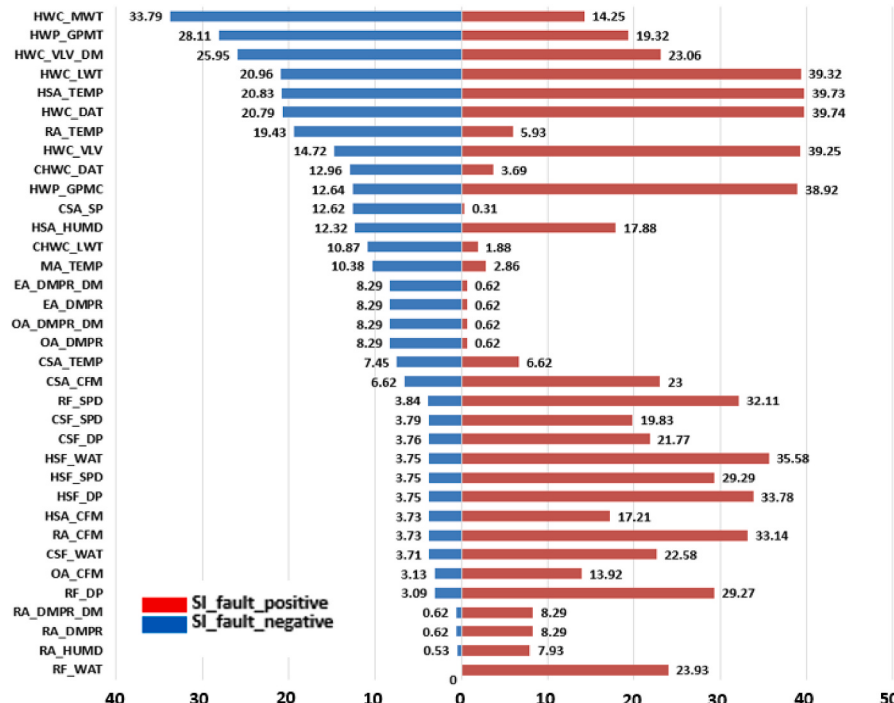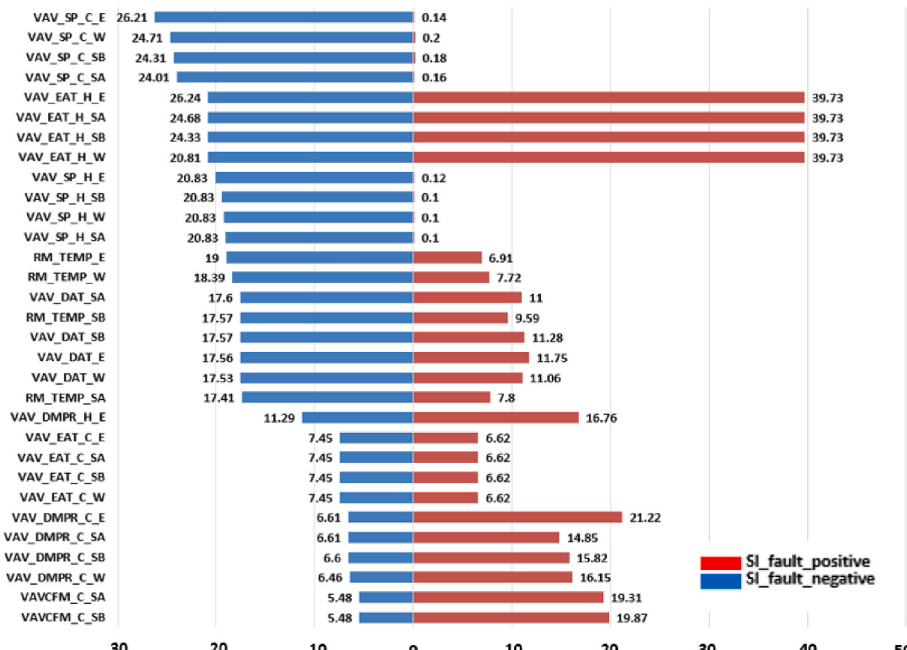
Fig. 7. SI_fault_positive and SI_fault_negative for the SensorBias_CSP fault.

(a)

(b)

Fig. 8. SI_fault_positive and SI_fault_negative for the VLVStuck_Heating fault: (a) measurements on the AHU side; (b) measurements on the VAV box side.

SI_fault_positive results (i.e., 39.74, 39.73 and 39.32, respectively). The measurements on the VAV box side are also sensitive to this fault. For example, the SI_fault_positive of entering temperature sensors on the hot deck is 39.73 for all four boxes, indicating that the inlet temperature higher than the baseline can be easily captured, when the stuck position is higher than the normal position. Similarly, when the stuck position is

higher than the normal position, the measurements on VAV mixing box air damper control signals are very sensitive as the SI_fault_positive values are from 14.85 to 21.22 for four VAV boxes, indicating the damper controllers try to mitigate the effects of the heating coil valve stuck. We will use the SI_fault_sum (i.e., sum of SI_fault_positive and SI_fault_negative) to analyze fault signatures in Section 4.4.

(3) F12: Fouling_Cooling_Airside fault case

The Fouling_Cooling_Airside fault is the airside fouling on the cooling water coil fault as described in Section 3.3.3. Fig. 9 illustrates the positive SI_fault and negative SI_fault of the measurements, in which the values are higher than 2, on the AHU side and the measurements on the VAV box side, respectively. There are 14 measurements that the SI_fault values are higher than the 2.

Compared to the actuator related faults, measurements are not very sensitive to the stationary component related faults. It can be seen that only 5 measurements (i.e., CSF_SPD, CSF_WAT, CSA_SP, HWP_GPMT, and CSF_DP) present relatively higher sensitivity to the fault compared to other measurements. Among them, the SI_fault_positive values on the measurements of CSF_SPD and CSF_WAT are 11.97 and 6.94, respectively, indicating that this fault can cause higher fan speed and corresponding fan energy consumption. We will use the SI_fault_sum (i.e., sum of SI_fault_positive and SI_fault_negative) to analyze fault signatures in Section 4.4.

(4) F14: CoolSeqUnstable fault case

The CoolSeqUnstable fault is the control parameter wrong setting fault as described in Section 3.3.4. Fig. 10 (a) and (b) illustrate the positive SI_fault and negative SI_fault, which the values are higher than 5 from the measurements on the AHU side and the measurements on the VAV box side, respectively.

It can be seen that most measurements from both the AHU side and the measurements on the VAV box side present highly sensitive values to this fault. For example, from the AHU side, the highest SI_fault_positive is 21.24 on the MA_TEMP measurement, indicating that the mixed air temperature sensor can easily collect positive symptoms (e.g., temperature is higher than the baseline value), when the fault occurs. This fault can also cause significant effects on the measurements of EA_DMPR_DM, OA_DMPR_DM, HWC_VLV_DM, HWC_VLV, and CSA_TEMP as SI_fault_negative or SI_fault_positive is higher than 18 as illustrated in Fig. 9 (a). This means that those measurements can more easily capture the fault's symptoms.

Many measurements on the VAV box side are sensitive to this fault as can be seen in Fig. 9 (b). Among them, the SI_fault_positive of the entering temperature sensors on the cold deck (e.g., VAV_EAT_C_E) for four VAV boxes presents the highest value (i.e., 18.31). This is the same as the CSA_TEMP on the AHU.

We will use the SI_fault_sum (i.e., sum of SI_fault_positive and SI_fault_negative) to analyze fault signatures in Section 4.4.

4.2. Analysis of the global measurement sensitivity index (SI_measurement_global)

The calculation of the SI_measurement_global is based on Eq (8) for all 15 types of faults in the VAV HVAC system. Figs. 11 and 12 illustrate the SI_measurement_global distributions for the measurements on the AHU side and on the VAV box side, respectively. To better illustrate the SI_measurement_global distribution, we split the bar chart into two parts according to whether the SI_measurement_global value is higher than 10 or not.

As shown in Fig. 11 (a), on the AHU side, the SI_measurement_global on 25 measurements is higher than 10. Among them, measurements on the hot deck present a relatively higher sensitivity considering all types of the faults. For example, the SI_measurement_global of the HWC_VLV_DM is 33.47, and SI_measurement_global of HSA_CFM is 21.26. In addition to the measurements on the hot deck, temperature measurements (e.g., CSA_TEMP, CHWC_DAT, MA_TEMP, and RA_TEMP) are highly sensitive to faults, i.e., the SI_measurement_global values for CSA_TEMP, CHWC_DAT, MA_TEMP, and RA_TEMP are 16.9, 16.8, 16.22 and 11.86, respectively. Furthermore, it is noticed that some metering measurements (e.g., CSF_WAT, HSF_WAT and RF_WAT) are not very
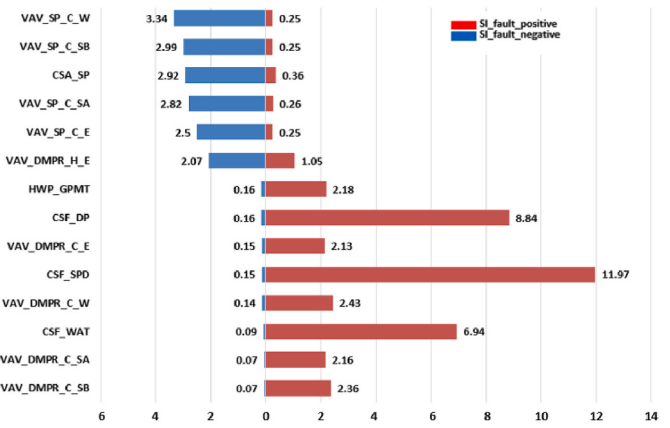
Fig. 9. SI_fault_positive and SI_fault_negative for the Fouling_Cooling_Airside fault.
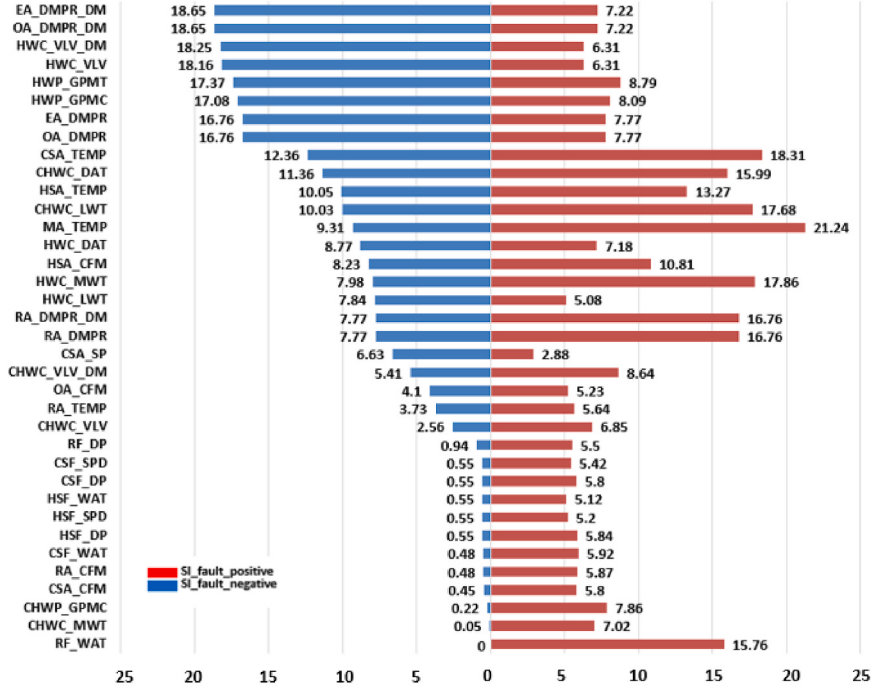
sensitive considering all types of faults, even though some metering measurements can be relatively sensitive to a certain type of a fault. This indicates that meter data is not good as an indicator if various types of faults are considered. Lastly, some measurements present very low sensitivity to faults. For example, the SI_measurement_global values for CHWC_EWT and HWC_EWT are 0, indicating that no fault in the AHU system can affect water supply temperature from the upstreaming chiller plants. Measurements on the humidities (i.e., HSA_HUMD, CSA_HUMD, and RA_HUMD) are not sensitive to faults because there is no there is not a humidity control loop in the system.

As shown in Fig. 12 (a), on the VAV box side, the SI_measurement_global on 28 measurements is higher than 10. Among them, the temperature measurements in the boxes demonstrate a relatively high sensitivity considering all types of faults. For example, the entering temperature sensors on the hot deck in each VAV box present equally high sensitivity (i.e., the SI_measurement_global value is 29.22 for VAV_EAT_H_E, VAV_EAT_H_SA, VAV_EAT_H_SB, and VAV_EAT_H_W). The entering temperature sensors on the cold deck in each VAV box also present equally high sensitivity (i.e., the SI_measurement_global value is 17.95 for VAV_EAT_C_E, VAV_EAT_C_SA, VAV_EAT_C_SB, and VAV_EAT_C_W). However, we noticed that the room temperature sensor is not very sensitive considering all types of faults, even though room temperature can be significantly affected by some certain types of faults. The SI_measurement_global values for four room temperature measurements (i.e., RM_TEMP_SA, RM_TEMP_SB, RM_TEMP_W, and RM_TEMP_E) are 9.33, 7.12, 6.76 and 5.97, respectively. Additionally, the measurements of mixing box damper control are not very sensitive in some VAV boxes. For example, the SI_measurement_global values for VAV_DMPR_C_SB, and VAV_DMPR_H_W are 7.94 and 8.34, respectively. This indicates that faults cannot significantly affect mixing box air damper controls. Hence, it will be relatively difficult to capture fault behaviors from assessing mixing box air damper controls in those VAV boxes.
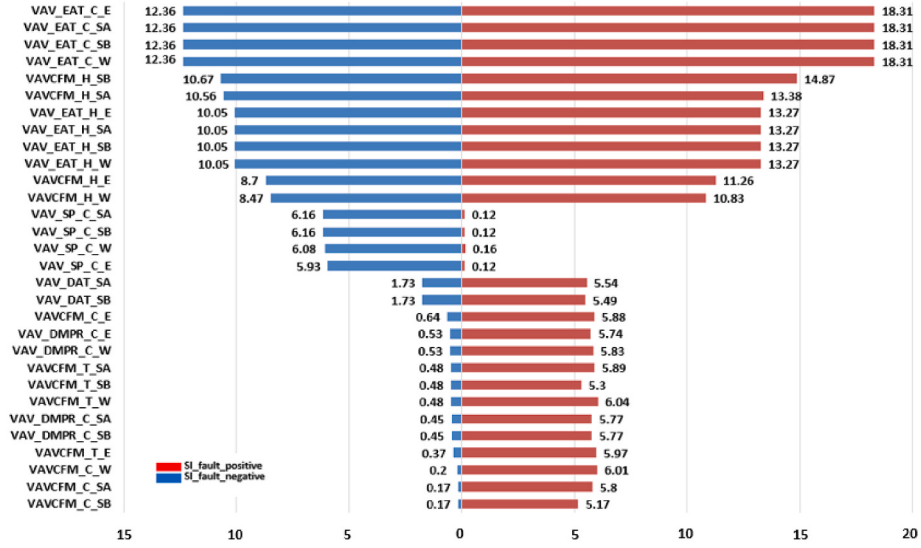
In summary, a total of 53 measurements from the AHU side and the VAV box side can be considered as relatively sensitive to faults (i.e., the SI_measurement_global value is higher than 10). Therefore, they can be considered as key performance indicators when deploying measurements and developing BASs.

4.3. Discussion of SI_fault and SI_measurement_global

When using the SI_fault and SI_measurement_global to analyze the measurement sensitivity, there are two things needing to be noticed. First, the calculations of the SI_fault and the SI_measurement_global include uncertainties. For example, the determination of occurrence of fault symptoms affects both indices. In this study, we used the "three-sigma empirical rule" to set the symptom occurrence threshold and

(a)

(b)
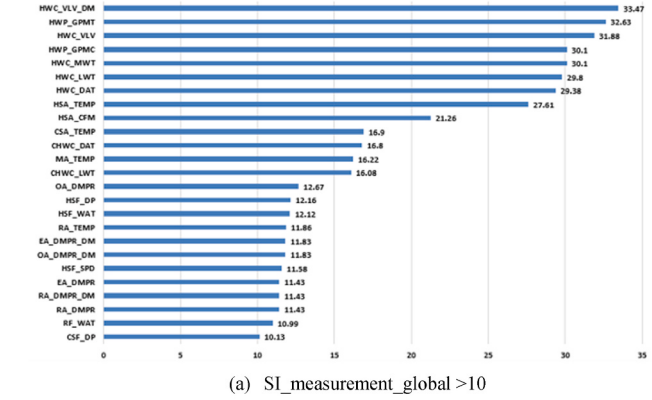
Fig. 10. SI_fault for the CoolSeqUnstable fault. (a) Measurements on the AHU side; (b) measurements on the VAV box side.

indicate observable symptoms. If the threshold is set to be low, the occurrence of fault symptoms will increase, resulting in a higher sensitivity of the measurement. Additionally, the determination of the fault occurrence probability distribution and the fault severity probability distributions affects the SIs as well. We employed expert knowledge in this study. However, we suggest the users update the SI distribution table in the Appendix when more information on the probability distributions is acquired. Second, in real practice, the location of a sensor may significantly affect the sensitivity. For example, the air flow sensor is recommended to be installed in the center of the duct to avoid measurement noises. In our study, we did not investigate how the
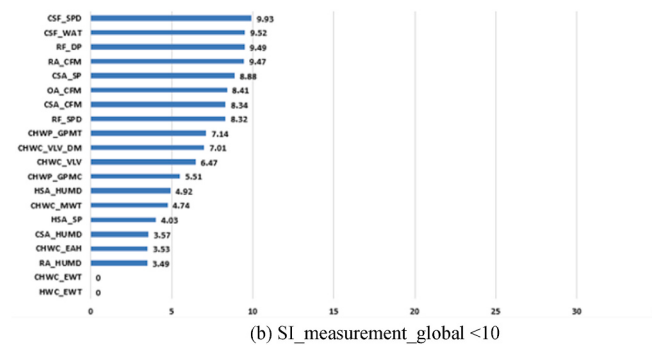
installation location of the sensor may affect the sensitivity because this is very hard to achieve in the simulation environment.

4.4. Usage case of SI_fault

A fault signature represents a set of fault symptoms that can be observed when a fault occurs. The ability of identification of a fault signature is very important for developing various FDD approaches. Various types of faults may manifest in distinct ways in terms of the sensitivities of various measurements, and hence present different sets of fault symptoms. Therefore, a FDD process is to accurately capture the
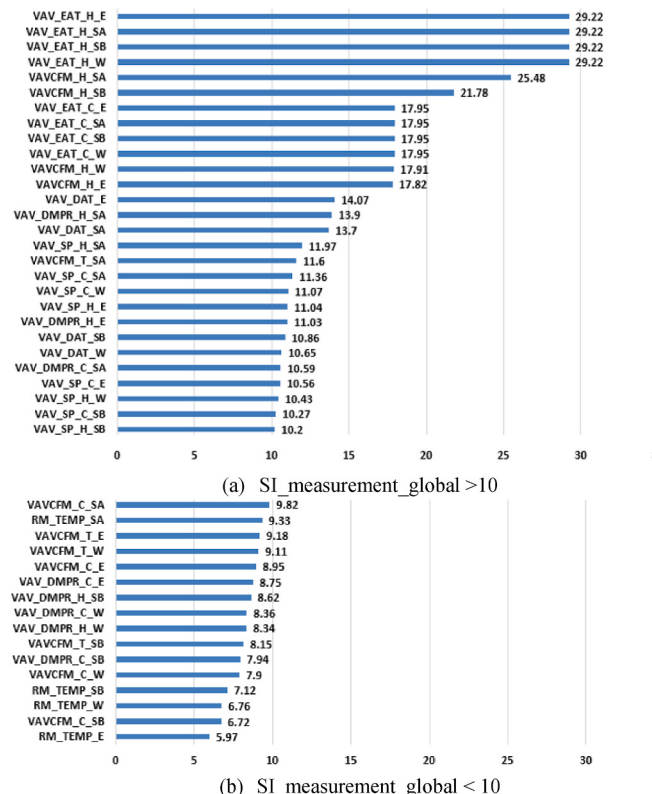
(a) SI_measurement_global >10
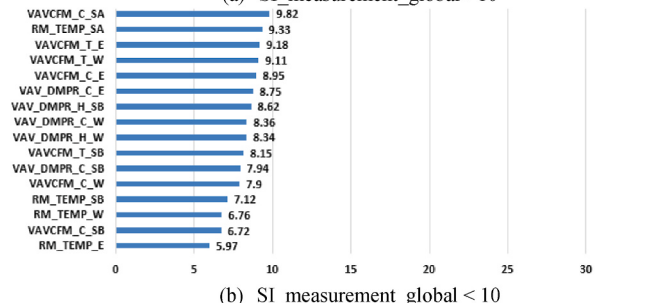
(b) SI_measurement_global <10

Fig. 11. SI_measurement_global for the AHU side.

(a) SI_measurement_global >10

(b) SI_measurement_global < 10

Fig. 12. SI_measurement_global for the VAV box side.

unique fault signature. On the one hand, if the fault signature is minor, it means that very few measurements are sensitive to a fault (i.e., fault symptoms can hardly be captured by the measurements). Consequently, the fault is hard to be detected. On the other hand, if various faults present a similar signature, i.e., similar sensitivities on the same measurements of multiple faults cause indistinguishable symptoms, it means that the faults can be hardly diagnosed.

In this study, we use SI_fault_sum (calculated from Eq. (7)) to analyze fault signature. Fig. 13 illustrates the heatmap of the SI_fault_sum of 89 measurements in terms of all 15 types of faults.

It can clearly be seen that compared with the sensor related faults (i. e., F1 to F4) and stationary component related faults (i.e., F10 to F13), the actuator related faults (i.e., F5 to F9) and the control setting related faults (i.e., F14 to F15) have more identifiable fault signatures because more measurements present higher SI_fault_sum. For example, for F6 (VLVStuck_Heating), the SI_fault_sum of 73 measurements (82% of all measurements) is higher than 10. For F3 (SensorBias_CSP), the SI_fault_sum for four measurements (i.e., VAV_SP_C_W, VAV_SP_C_SB, VAV_SP_C_SA, and VAV_SP_C_E) in four VAV boxes are higher than 10, and can be used as the signatures to indicate this fault. For F14 (Cool-SeqUnstable), the SI_fault_sum of 33 measurements (37% of all measurements) is higher than 10. Contrarily, for the F12 (Fouling_Cooling_Airside) fault, only one measurement (i.e., CSF_SPD) shows the SI_fault_sum value is higher than 10 (i.e., 12). This indicates that this fault could be very difficult to detect using existing measurements in this paper, i.e., the fault has a low detectability.

Additionally, it should be noticed that there are fault types showing the closed SI_fault_sum values on certain measurements, resulting in low diagnosability if those measurements are used for diagnosing those faults. For example, for the F4 (SensorBias_HSP) fault, the SI_fault_sum values of HSF_DP, HSF_SPD, HSF_WAT, and HWC_DAT are 12.5, 12.5, 12.5, and 11.3, respectively. For the F8 (DMPRStuck_Hot) fault, the SI_fault_sum values for those four measurements are 8.8, 12.8, 12.4, and 14.7, respectively. This indicates that the FDD tool cannot distinguish the F4 fault from the F8 fault only using the above four measurements.

In summary, the developed SIs can be used to effectively evaluate fault signatures, and support the development of FDD tools.

5. Conclusions and future work

In this study, we propose two novel sensitive indices, namely the SI of a fault (SI_fault) and the global measurement SI (SI_measurement_global). The SI_fault quantifies the sensitivity of a measurement to a specific type of fault. The SI_measurement_global quantifies the sensitivity of a measurement considering various types of faults. The developed SIs contains multiple elements including symptom occurrence probability (SOP) distributions, fault severity probability distributions, and fault occurrence probability distributions to enhance the interpretability and scalability.

The developed SIs have higher interpretability because it well captures the system's behaviors when a fault occurs. At the same time, the developed SIs are more scalable because fault severity probability distributions and fault occurrence probability can be updated when more knowledge about the faults is obtained.

We employed interval data generated from the HVACSIM+ simulation enviroment to evaluate the sensitivity of various measurements under common faults in a dual-duct VAV HVAC system. A total of 15 common fault types under different severity levels were simulated, resulting in 55 fault cases. For each fault case, a one-year of system's faulty operation data were obtained so that a comprehensive evaluation of the measurement sensitivity under various system operation conditions can be achieved. Additionally, the system wide measurement sensitivity analysis (from the upstream AHU to the downstream VAV boxes) provides a broader view of the measurement sensitivities.

In the future, we plan to extend the study in four directions. First, we will apply the developed method and the SIs to other types of HVAC

	F1	F2	F3	F4	F5	F6	F7	F8	F9	F10	F11	F12	F13	F14	F15
OA_CFM	3.3	1.1	0.76	0.79	13	17	8.2	5.7	11	3.4	2.3	1.2	1.8	9.3	1.9
OA_DMPR	7	0.43	0.45	0.41	12	8.9	1.9	1.1	43	0.93	0.95	1.2	0.93	25	0.99
OA_DMPR_DM	7	0.43	0.45	0.42	12	8.9	1.9	1.1	18	0.93	0.95	1.2	0.93	26	0.99
MA_TEMP	12	0.83	1	0.73	32	13	5.6	1.9	16	3.3	1.7	2.1	1.7	31	1.9
RA_CFM	5.9	1.4	0.84	0.82	18	37	12	7.6	10	6.7	2.4	1.6	1.8	6.3	2
RA_DMPR	7	0.43	0.45	0.41	12	8.9	1.9	1.1	18	0.93	0.95	1.2	0.93	25	0.99
RA_DMPR_DM	7	0.43	0.45	0.41	12	8.9	1.9	1.1	18	0.93	0.95	1.2	0.93	25	0.99
RA_HUMD	2.6	0.39	0.4	0.4	12	8.5	1.7	1.1	8.1	2.7	0.93	0.87	0.88	1.2	0.94
RA_TEMP	2.7	1.1	0.88	0.88	19	25	22	2.8	11	5.5	2	2	2	9.4	8.4
RF_DP	5.7	1.6	1	1.1	11	32	13	7.8	7.2	4.6	3	2.6	2.4	6.4	2.5
RF_SPD	6.2	1.1	0.6	0.6	16	36	13	6.8	12	6	1.9	1.7	1.4	5	1.5
RF_WAT	3.1	1.2	0.91	0.92	18	24	8.7	4	4.3	6.4	2.5	1.8	2.1	16	2.4
EA_DMPR	7	0.43	0.45	0.41	12	8.9	1.9	1.1	18	0.93	0.95	1.2	0.93	25	0.99
EA_DMPR_DM	7	0.43	0.45	0.42	12	8.9	1.9	1.1	18	0.93	0.95	1.2	0.93	26	0.99
HSA_SP	2.5	0.2	0.19	0.21	0.33	4	0.84	0.83	24	0.41	0.41	0.44	0.43	5.4	0.56

|	F1	F2	F3	F4	F5	F6	F7	F8	F9	F10	F11	F12	F13	F14	F15
HSA_CFM	3.3	1.2	1	1	1.5	21	20	57	16	2.2	2.6	2.3	2.3	19	23
HSA_TEMP	2.6	0.57	0.54	0.49	11	61	1.9	1.4	13	1.2	3.2	1.1	1.1	23	49
HSF_DP	5.4	1.5	0.94	12	18	38	11	8.8	30	6.8	2.6	1.7	9	6.4	2.4
HSF_SPD	5.2	1.2	0.86	12	18	33	11	13	30	6.5	2.2	1.4	8.4	5.8	2.2
HSF_WAT	5.3	1.4	0.92	12	17	39	13	12	30	6.7	2.5	1.9	9	5.7	2.3
CSA_SP	3.3	0.88	0.64	0.76	17	13	1.4	1.8	24	6.3	1.7	3.3	1.7	9.5	3.1
CSA_HUMD	2.9	0.41	0.42	0.43	14	4.9	1.4	1.3	6.2	0.93	0.97	0.93	0.94	1.9	1.1
CSA_CFM	5.7	1.1	0.73	0.71	18	30	13	3.6	6.8	6.4	1.7	1.2	1.6	6.2	1.8
CSA_TEMP	6.3	1	0.97	0.99	37	14	3.8	2.3	16	7.8	2.2	2.1	2.3	31	3
CSF_DP	5.7	1.2	3.8	0.93	18	26	12	5.2	24	6.6	2.5	9	2.1	6.3	2.1
CSF_SPD	5	1.1	5.2	0.87	18	24	9.6	5.2	28	6.5	2.4	12	2	6	2.1
CSF_WAT	5.5	1.2	3.1	0.79	18	26	13	5.1	21	6.5	2.1	7	1.7	6.4	2
HWC_DAT	3.9	17	0.49	11	11	61	1.6	15	23	1.1	3.1	1.1	5.1	16	49
HWC_EWT	0	0	0	0	0	0	0	0	0	0	0	0	0	0	0

	F1	F2	F3	F4	F5	F6	F7	F8	F9	F10	F11	F12	F13	F14	F15
HWC_MWT	10	9.6	0.76	0.85	13	48	12	21	15	1.2	34	1.4	1.2	26	44
HWC_VLV	9.2	11	0.62	2.4	15	54	9.5	19	18	1.1	3.3	1.1	1.8	24	51
HWC_VLV_DM	9.2	11	0.62	2.4	15	49	9.5	19	18	1.1	3.3	1.1	1.8	25	57
HWP_GPMC	9.6	13	0.71	2.5	12	52	14	23	16	1.3	2.7	1.5	1.4	25	42
HWP_GPMT	9.9	14	1.1	2.8	13	47	14	24	17	2.1	88	2.3	2.3	26	44
CHWC_DAT	17	0.87	1.1	0.87	38	17	2.7	2	22	7.6	2	2.2	1.9	27	2.2
CHWC_EAH	2.3	0.38	0.39	0.4	8.3	5	1.2	1.1	6.4	0.99	0.96	0.85	0.9	3.1	0.85
CHWC_EWT	0	0	0	0	0	0	0	0	0	0	0	0	0	0	0
CHWC_LWT	16	0.67	1	0.69	41	13	3.7	1.7	20	3.7	1.6	1.9	1.5	28	1.7
CHWC_MWT	0.78	0.18	0.12	0.11	31	4.2	0.44	0.46	5.5	8	0.25	0.42	0.25	7.1	0.36
CHWC_VLV	3.7	0.23	0.21	0.21	38	3.8	0.95	0.61	8.6	2.9	0.47	0.7	0.46	9.4	0.54
CHWC_VLV_DM	3.7	0.23	0.21	0.21	21	3.8	0.95	0.61	8.6	2.9	0.46	0.7	0.47	14	0.54
CHWP_GPMC	3.5	0.14	0.11	0.08	34	3.7	1.2	0.54	8.9	0.24	0.19	0.77	0.19	8.1	0.29
CHWP_GPMT	1.4	0.36	0.36	0.36	37	0.64	0.98	0.66	6.6	83	0.81	0.77	0.81	9.2	0.9

	F1	F2	F3	F4	F5	F6	F7	F8	F9	F10	F11	F12	F13	F14	F15
VAV_DAT_W	1.2	0.67	0.55	0.56	18	29	1.3	1.2	9.7	5.9	1.8	1.2	1.3	6	14
VAV_SP_C_W	5.2	1.3	16	1	18	25	5.4	2.8	23	7	2.4	3.6	2.3	6.2	2.6
VAV_SP_H_W	2.6	0.59	0.37	34	0.93	19	13	34	23	0.83	1.2	0.85	0.83	4	0.78
VAV_DMPR_C_W	4.1	1.2	1.1	0.87	18	23	2.3	2.3	18	6.3	2	2.6	2	6.4	2.2
VAV_DMPR_H_W	2.4	1.1	0.85	17	6.1	20	1.8	1.6	19	3.5	2.3	1	1.9	4.6	2
VAVCFM_C_W	4.4	1.2	0.92	0.96	18	22	2.2	2.2	4.3	6.7	2.2	1.7	2.2	6.2	2.8
VAVCFM_H_W	3.3	1.3	1.1	1.1	1.5	21	1.8	2.1	15	2.4	2.7	2.4	2.3	19	24
VAVCFM_T_W	5.3	1.4	1	1	18	33	2.6	2.5	9.8	6.9	2.9	1.9	2.3	6.5	2.5
VAV_EAT_C_W	17	1	0.97	0.99	37	14	3.8	2.3	16	7.8	2.2	2.1	2.3	31	3
VAV_EAT_H_W	2.6	17	0.54	0.49	11	61	1.9	1.4	13	1.2	3.2	1.1	1.1	23	49
RM_TEMP_SB	2.2	0.93	0.79	0.76	19	27	1.5	1.6	11	7	2.1	2	1.7	4.6	1.9
VAV_DAT_SB	1.1	0.85	0.47	0.47	19	29	1.3	0.97	9.8	5.8	1.4	1.1	1.1	7.2	15
VAV_SP_C_SB	5.3	1.2	16	0.83	18	25	3.5	2.4	23	6.5	2	3.2	1.8	6.3	2.1
VAV_SP_H_SB	2.5	0.55	0.34	32	0.69	20	14	35	23	0.73	1.2	0.78	0.74	3.8	0.75

	F1	F2	F3	F4	F5	F6	F7	F8	F9	F10	F11	F12	F13	F14	F15
VAV_DMPR_H_SB	3	1	0.81	19	5.9	22	1.8	1.8	20	3.4	2.4	0.99	1.8	4.7	1.9
VAVCFM_C_SB	4.8	0.8	0.58	0.65	16	25	1.9	1.6	5.2	6.2	1.6	1.1	1.5	5.3	1.6
VAVCFM_H_SB	3.6	1.3	1.1	1.2	1.5	20	2.1	2.3	17	2.5	2.9	2.6	2.5	26	30
VAVCFM_T_SB	5.7	1	0.69	0.76	17	34	2.4	2	13	6.5	2.3	1.4	1.7	5.8	1.9
VAV_EAT_C_SB	17	1	0.97	0.99	37	14	3.8	2.3	16	7.8	2.2	2.1	2.3	31	3
VAV_EAT_H_SB	2.6	17	0.54	0.49	11	61	1.9	1.4	13	1.2	3.2	1.1	1.1	23	49
RM_TEMP_SA	2.2	0.75	0.72	0.73	19	25	44	11	9.3	6	2.1	1.6	1.6	4.4	1.8
VAV_DAT_SA	1.1	0.81	0.49	0.5	19	29	37	23	9.7	5.7	1.4	1.1	1.1	7.3	14
VAV_SP_C_SA	5.2	1.2	16	0.81	18	24	21	9.1	23	6.5	1.9	3.1	1.8	6.3	2
VAV_SP_H_SA	2.5	0.55	0.38	32	0.79	19	22	55	23	0.84	1.2	0.86	0.81	4.7	0.75
VAV_DMPR_C_SA	4.2	0.95	0.79	0.75	18	21	48	12	18	6	1.7	2.2	1.7	6.2	1.9
VAV_DMPR_H_SA	2.7	0.95	0.78	26	12	26	23	65	20	5.8	2.1	1.2	1.7	4.4	1.9
VAVCFM_C_SA	4.4	0.99	0.69	0.72	18	25	44	13	4.8	6.4	1.8	1.2	1.6	6	1.8
VAVCFM_H_SA	3.5	1.3	1.1	1.1	1.4	20	23	66	17	2.5	2.9	2.6	2.5	24	29

	F1	F2	F3	F4	F5	F6	F7	F8	F9	F10	F11	F12	F13	F14	F15
VAV_EAT_C_SA	17	1	0.97	0.99	37	14	3.8	2.3	16	7.8	2.2	2.1	2.3	31	3
VAV_EAT_H_SA	2.6	17	0.54	0.49	11	61	1.9	1.4	13	1.2	3.2	1.1	1.1	23	49
RM_TEMP_E	2.1	0.61	0.55	0.56	18	26	1.4	1.3	9.5	5.1	1.7	1.2	1.2	3.9	1.3
VAV_DAT_E	2.3	2.2	0.62	0.62	21	29	1.7	1.4	11	5.7	2	1.4	1.4	7.1	23
VAV_SP_C_E	5.5	1.5	16	0.87	18	26	4.9	2.4	23	6.6	2.1	2.8	1.9	6	2.1
VAV_SP_H_E	2.8	0.61	0.32	34	0.94	20	16	37	24	0.73	1.1	0.75	0.79	5	0.69
VAV_DMPR_C_E	4.5	1.3	1.7	0.88	18	28	2.2	2	18	6.3	2.1	2.3	2	6.3	2.3
VAV_DMPR_H_E	7.2	1.6	1.1	22	3.1	28	3.1	2.7	22	2.9	3.1	2.4	2.4	5.2	3.6
VAVCFM_C_E	5.4	1.5	0.89	1	18	27	2.5	2.2	7.5	6.8	2.5	1.9	2.2	6.5	4.1
VAVCFM_H_E	3.4	1.4	1	1.1	1.8	21	1.9	2.2	12	2.3	2.7	2.4	2.4	20	23
VAVCFM_T_E	5.3	1.7	0.94	0.97	19	39	2.5	2.1	9.5	6.8	2.6	1.9	2.2	6.3	2.4
VAV_EAT_C_E	17	1	0.97	0.99	37	14	3.8	2.3	16	7.8	2.2	2.1	2.3	31	3
VAV_EAT_H_E	2.6	17	0.54	0.49	11	61	1.9	1.4	13	1.2	3.2	1.1	1.1	23	49

Fig. 13. Heatmap of the SI_fault_sum.

systems to build a comprehensive measurement SI distribution system. Secondly, we will evaluate the measurement sensitivity under various incipient faults, where fault transient symptoms on various measurements can be different from steady faulty operations investigated in the current study. Thirdly, we will evaluate the measurement sensitivity under various simultaneous faults. Lastly, we will investigate more software related faults including more fault types and more severity levels.

CRediT authorship contribution statement

Yimin Chen: Writing – original draft, Supervision, Methodology, Formal analysis, Data curation, Conceptualization. **Zhelun Chen:** Writing – review & editing, Software, Formal analysis, Data curation. **Guanjing Lin:** Writing – review & editing, Data curation. **Yun Zhang:** Writing – review & editing, Formal analysis. **Shi Ye:** Writing – review & editing, Visualization, Software.

Declaration of competing interest

The authors declare that they have no known competing financial interests or personal relationships that could have appeared to influence the work reported in this paper.

Data availability

I will attach the data.

Acknowledgments

Appendix A. Supplementary data

Supplementary data to this article can be found online at https://doi.org/10.1016/j.buildenv.2024.111683.

References

[1] 2012 Commercial Buildings Energy Consumption Survey: Energy Usage Summary, Energy Information Administration, U.S., Washington, DC, 2016. https://www.eia.

gov/consumption/commercial/reports/2012/energyusage/. (Accessed 25 January 2021).

[2] S. Katipamula, M.R. Brambley, Methods for fault detection, diagnostics, and prognostics for building systems—a review, Part I, HVAC R Res. 11 (2005) 3–25, https://doi.org/10.1080/10789669.2005.10391123.

[3] Y. Chen, Z. Chen, G. Lin, J. Wen, J. Granderson, A simulation-based method to analyze fan coil unit fault impacts, in: ASHRAE Trans., ASHRAE, Toronto, Canada, 2022, p. 210. https://www.ashrae.org/technical-resources/ashrae-transactions.

[4] S. Deshmukh, L. Glicksman, L. Norford, Case study results: fault detection in air-handling units in buildings, Adv. Build. Energy Res. 14 (2020) 305–321.

[5] R. Zhang, T. Hong, Modeling of HVAC operational faults in building performance simulation, Appl. Energy 202 (2017) 178–188, https://doi.org/10.1016/j.apenergy.2017.05.153.

[6] W. Kim, S. Katipamula, A review of fault detection and diagnostics methods for building systems, Sci. Technol. Built Environ. 24 (2018) 3–21, https://doi.org/10.1080/23744731.2017.1318008.

[7] Z. Shi, W. O'Brien, Development and implementation of automated fault detection and diagnostics for building systems: a review, Autom. ConStruct. 104 (2019) 215–229, https://doi.org/10.1016/j.autcon.2019.04.002.

[8] Y. Yu, D. Woradechjumroen, D. Yu, A review of fault detection and diagnosis methodologies on air-handling units, Energy Build. 82 (2014) 550–562, https://doi.org/10.1016/j.enbuild.2014.06.042.

[9] Z. Chen, Z. O'Neill, O. Pradhan, T. Yang, X. Lu, G. Lin, S. Miyata, S. Lee, C. Shen, R. Chiosa, M.S. Piscitelli, A. Capozzoli, F. Hengel, A. Kührer, M. Pritoni, W. Liu, J. Clauß, Y. Chen, T. Herr, A review of data-driven fault detection and diagnostics for building HVAC systems, Appl. Energy 339 (2023) 121030, https://doi.org/10.1016/j.apenergy.2023.121030.

[10] H.H. Hosamo, H.K. Nielsen, D. Kraniotis, P.R. Svennevig, K. Svidt, Digital Twin framework for automated fault source detection and prediction for comfort performance evaluation of existing non-residential Norwegian buildings, Energy Build. 281 (2023) 112732, https://doi.org/10.1016/j.enbuild.2022.112732.

[11] X. Xie, J. Merino, N. Moretti, P. Pauwels, J.Y. Chang, A. Parlikad, Digital twin enabled fault detection and diagnosis process for building HVAC systems, Autom. ConStruct. 146 (2023) 104695, https://doi.org/10.1016/j.autcon.2022.104695.

[12] Y. Chen, Data-Driven Whole Building Fault Detection and Diagnosis, Drexel University, 2019. Ph.D. https://www.proquest.com/docview/2275119448/abstract/A8D5FCEB15DC48CAPQ/1. (Accessed 16 August 2023).

[13] C. Yan, S. Wang, F. Xiao, D. Gao, A multi-level energy performance diagnosis method for energy information poor buildings, Energy 83 (2015) 189–203, https://doi.org/10.1016/j.energy.2015.02.014.

[14] F. Xiao, C. Fan, Data mining in building automation system for improving building operational performance, Energy Build. 75 (2014) 109–118, https://doi.org/10.1016/j.enbuild.2014.02.005.

[15] Y. Chen, J. Wen, L.J. Lo, Using weather and schedule based pattern matching and feature based PCA for whole building fault detection — Part I development of the method, ASME J. Eng. Sustain. Build. Cities (2021) 1–23, https://doi.org/10.1115/1.4052729.

[16] S. Yoon, Building digital twinning: data, information, and models, J. Build. Eng. 76 (2023) 107021, https://doi.org/10.1016/j.jobe.2023.107021.

[17] T.M. Rossi, J.E. Braun, A statistical, rule-based fault detection and diagnostic method for vapor compression air conditioners, HVAC R Res. 3 (1997) 19–37.

[18] M.S. Breuker, J.E. Braun, Common faults and their impacts for rooftop air conditioners, HVAC R Res. 4 (1998) 303–318, https://doi.org/10.1080/10789669.1998.10391406.

[19] I.B.D. McIntosh, J.W. Mitchell, W.A. Beckman, Fault detection and diagnosis in chillers–part I: model development and application/Discussion, Build. Eng. 106 (2000) 268.

[20] M.C. Comstock, J.E. Braun, E.A. Groll, The sensitivity of chiller performance to common faults, HVAC R Res. 7 (2001) 263–279, https://doi.org/10.1080/10789669.2001.10391274.

[21] B. Chen, J.E. Braun, Simple rule-based methods for fault detection and diagnostics applied to packaged air conditioners/Discussion, Build. Eng. 107 (2001) 847.

[22] F. Xiao, C. Zheng, S. Wang, A fault detection and diagnosis strategy with enhanced sensitivity for centrifugal chillers, Appl. Therm. Eng. 31 (2011) 3963–3970, https://doi.org/10.1016/j.applthermaleng.2011.07.047.

[23] S.-H. Cho, H.-C. Yang, M. Zaheer-uddin, B.-C. Ahn, Transient pattern analysis for fault detection and diagnosis of HVAC systems, Energy Convers. Manag. 46 (2005) 3103–3116, https://doi.org/10.1016/j.enconman.2005.02.012.

[24] Y. Chen, S. Huang, D. Vrabie, A simulation based approach to impact assessment of physical faults: large commercial building hvac case study, in: 2018 Build. Perform. Model. Conf. SimBuild Co-Organ. ASHRAE IBPSA-USA Chic, 2018. IL USA.

[25] I. Bellanco, F. Belío, M. Vallés, R. Gerber, J. Salom, Common fault effects on a natural refrigerant, variable-speed heat pump, Int. J. Refrig. 133 (2022) 259–266, https://doi.org/10.1016/j.ijrefrig.2021.10.017.

[26] D. Li, Y. Zhou, G. Hu, C.J. Spanos, Optimal sensor configuration and feature selection for AHU fault detection and diagnosis, IEEE Trans. Ind. Inf. 13 (2017) 1369–1380, https://doi.org/10.1109/TII.2016.2644669.

[27] H. Han, B. Gu, T. Wang, Z.R. Li, Important sensors for chiller fault detection and diagnosis (FDD) from the perspective of feature selection and machine learning, Int. J. Refrig. 34 (2011) 586–599, https://doi.org/10.1016/j.ijrefrig.2010.08.011.

[28] K. Yan, L. Ma, Y. Dai, W. Shen, Z. Ji, D. Xie, Cost-sensitive and sequential feature selection for chiller fault detection and diagnosis, Int. J. Refrig. 86 (2018) 401–409.

[29] W. Gou, Z. Ren, H. Chen, L. Xing, Z. Zhou, X. Xia, J. Shi, Experimental research on the performance and parameters sensitivity analysis of variable refrigerant flow system with common faults imposed in heating mode, Energy Build. 278 (2023) 112624, https://doi.org/10.1016/j.enbuild.2022.112624.

[30] M. Kim, S.H. Yoon, W.V. Payne, P.A. Domanski, Cooling Mode Fault Detection and Diagnosis Method for a Residential Heat Pump, U.S. DEPARTMENT OF COMMERCE, NATIONAL INSTITUTE OF STANDARDS AND TECHNOLOGY, Gaithersburg, Maryland U.S., 2008.

[31] X. Lu, Z. O'Neill, Y. Li, F. Niu, A novel simulation-based framework for sensor error impact analysis in smart building systems: a case study for a demand-controlled ventilation system, Appl. Energy 263 (2020) 114638.

[32] J. Granderson, G. Lin, Y. Chen, A. Casillas, J. Wen, Z. Chen, P. Im, S. Huang, J. Ling, A labeled dataset for building HVAC systems operating in faulted and fault-free states, Sci. Data 10 (2023) 342, https://doi.org/10.1038/s41597-023-02197-w.

[33] H. Cheung, J.E. Braun, Simulation of fault impacts for vapor compression systems by inverse modeling. Part I: component modeling and validation, HVAC R Res. 19 (2013) 892–906, https://doi.org/10.1080/10789669.2013.824800.

[34] Y. Chen, J. Wen, J. Granderson, A simulation-based evaluation of fan coil unit fault effects, Energy Build. 263 (2022) 112041, https://doi.org/10.1016/j.enbuild.2022.112041.

[35] Y. Chen, J. Wen, O. Pradhan, L.J. Lo, T. Wu, Using discrete Bayesian networks for diagnosing and isolating cross-level faults in HVAC systems, Appl. Energy 327 (2022) 120050, https://doi.org/10.1016/j.apenergy.2022.120050.

[36] Y. Chen, J. Wen, L.J. Lo, Using weather and schedule based pattern matching and feature based PCA for whole building fault detection — Part II field evaluation, ASME J. Eng. Sustain. Build. Cities (2021) 1–16, https://doi.org/10.1115/1.4052730.

[37] X. Lu, Y. Fu, Z. O'Neill, J. Wen, A holistic fault impact analysis of the high-performance sequences of operation for HVAC systems: modelica-based case study in a medium-office building, Energy Build. 252 (2021) 111448.

[38] S. Li, J. Wen, Application of pattern matching method for detecting faults in air handling unit system, Autom. ConStruct. 43 (2014) 49–58, https://doi.org/10.1016/j.autcon.2014.03.002.

[39] X. Liang, T. Hong, G.Q. Shen, Improving the accuracy of energy baseline models for commercial buildings with occupancy data, Appl. Energy 179 (2016) 247–260, https://doi.org/10.1016/j.apenergy.2016.06.141.

[40] J. Kim, K. Trenbath, J. Granderson, Y. Chen, E. Crowe, H. Reeve, et al., Research challenges and directions in HVAC fault prevalence, Sci Technol Built Environ 27 (2021) 624–640, https://doi.org/10.1080/23744731.2021.1898243.

[41] D.R. Clark, W.B. May, HVACSIM+ Building Systems and Equipment Simulation Program - User's Guide, National Bureau of Standards, Building Equipment Division, Washington, DC, 1985. https://www.osti.gov/biblio/6127383. (Accessed 20 November 2021).

[42] Z. Chen, J. Wen, A.J. Kearsley, A. Pertzborn, Evaluating the performance of an Inexact Newton method with a preconditioner for dynamic building system simulation, J. Build. Perform. Simul. 15 (2022) 112–127, https://doi.org/10.1080/19401493.2021.2007285.

[43] J. Wen, S. Pourarian, X. Yang, X. Li, NIST 10D243 Tools for Evaluating Fault Detection and Diagnostic Methods for HVAC Secondary Systems of a Net Zero Building, the US National Institute of Standard & Technology, 2015. Gaithersburg, MD US, https://www.researchgate.net/profile/Jin-Wen-12/publication/337946061_NIST10D243_FinalReport_-Tools_for_Evaluating_Fault_Detection_and_Diagnostic_Methods_for_HVAC_Secondary_Systems_of_a_Net_Zero_Building/links/5df73f11299bf10bc35f1163/NIST10D243-FinalReport-Tools-for-Evaluating-Fault-Detection-and-Diagnostic-Methods-for-HVAC-Secondary-Systems-of-a-Net-Zero-Building.pdf. (Accessed 25 January 2021).

[44] Y. Chen, G. Lin, E. Crowe, J. Granderson, Development of a unified taxonomy for HVAC system faults, Energies 14 (2021) 5581, https://doi.org/10.3390/en14175581.

[45] K. Roth, D. Westphalen, P. Llana, M. Feng, The energy impact of faults in U.S. Commercial buildings, in: Int. Refrig. Air Cond. Conf., IN, Purdue University, West Lafayette, 2004.

[46] J. Schein, S.T. Bushby, N.S. Castro, J.M. House, A rule-based fault detection method for air handling units, Energy Build. 38 (2006) 1485–1492, https://doi.org/10.1016/j.enbuild.2006.04.014.

[47] S. Wang, F. Xiao, AHU sensor fault diagnosis using principal component analysis method, Energy Build. 36 (2004) 147–160, https://doi.org/10.1016/j.enbuild.2003.10.002.

[48] Y. Zhao, J. Wen, S. Wang, Diagnostic Bayesian networks for diagnosing air handling units faults – Part II: faults in coils and sensors, Appl. Therm. Eng. 90 (2015) 145–157, https://doi.org/10.1016/j.applthermaleng.2015.07.001.

[49] Y. Zhao, J. Wen, F. Xiao, X. Yang, S. Wang, Diagnostic Bayesian networks for diagnosing air handling units faults – part I: faults in dampers, fans, filters and sensors, Appl. Therm. Eng. 111 (2017) 1272–1286, https://doi.org/10.1016/j.applthermaleng.2015.09.121.

[50] Y. Li, Z. O'Neill, An innovative fault impact analysis framework for enhancing building operations, Energy Build. 199 (2019) 311–331.

[51] E. Mills, Building commissioning: a golden opportunity for reducing energy costs and greenhouse gas emissions in the United States, Energy Effic 4 (2011) 145–173, https://doi.org/10.1007/s12053-011-9116-8.

[52] K. Mařík, J. Rojíček, P. Stluka, J. Vass, Advanced HVAC control: theory vs. Reality, IFAC Proc 44 (2011) 3108–3113, https://doi.org/10.3182/20110828-6-IT-1002.03085.